Synthesis and characterization of Fe-doped TiO_2 on fiberglass cloth for

the wastewater treatment reactor

By

Faysal Ahmed

A thesis submitted in partial fulfillment of the requirements for the

Degree of

MASTER OF APPLIED SCIENCE

in the

Department of Mechanical Engineering

University of Victoria

Supervisory Committee

Synthesis and characterization of Fe-doped TiO_2 on fiberglass cloth for the wastewater treatment reactor

By

Faysal Ahmed

Supervisory Committee

Co-Supervisors
Dr. Rodney Herring (Department of Mechanical Engineering)
Dr. Keivan Ahmadi (Department of Mechanical Engineering)

Abstract

The photocatalytic wastewater treatment facility presented in this thesis is a promising economic green technology that can degrade wastewater's organic and ammonia pollutants, which produce environmentally sensitive products like CO_2, H_2O, Nitrates, etc. that can be captured and used in many biological and engineering ways. Previous advances used for this research was determining the importance of cleaning the photocatalytic nanocrystals, Fe-TiO_2, as one of the revolutionary improvements that expose and maximizes the active surface of the photocatalytic nanocrystals to the pollutants enabling the strong oxidants produced by the absorption of a photon, excitation of an electron and positive hole to produce oxidants on the surface of the nanocrystals. The oxidants indiscriminately produce CO_2 and H_2O from living and non-living organic matter to obtain near ~100% clean water. This research focused on taking the next steps in the development of a wastewater cleaning facility tested in our laboratory. An important step involved coating Fe-TiO_2 crystals onto flexible, strong, fiber-glass cloth using a sol-gel processing method. Success was found in this research by applying the coated fiberglass cloth into a photoreactor aimed to clean a large amount of water rather than the laboratory scale.

Table of Contents

List of Figures

List of Tables

Abbreviations

AOPs	Advanced Oxidation Processes
CAD	Computer-Aided Design
CB	Conduction Band
CTE	Coefficient of Thermal Expansion
DC	Direct Current
EDS	Energy-Dispersive X-ray spectroscopy
LED	Light Emitting Diode
LSPR	Localized Surface Plasmon Resonance
MO	Methyl Orange
NP	Nano Particles
SEM	Secondary Electron Microscopy
SPR	Surface plasmon Resonance
TTIP	Titanium Tetraisopropoxide
VB	Valance Band
XRD	X-ray Diffractometer

Acknowledgments

I would like to express my sincere thanks to my supervisor and mentor, Dr. Rodney Herring, for giving me the opportunity to work on such a fascinating project. Thank you for your guidance, support, and fruitful discussions throughout this research work and for supporting me during my study. I'm grateful and consider myself fortunate for having the chance to learn from you. Working with you has been a great life experience and it has made me a better researcher and most importantly a better person. I really admire your positive attitude and great passion for your work and life. I learned a lot from you and grateful to you for believing in me.

Next, I would like to thank Dr. Barbara Sawicki and Jerzy A. Sawicki, for their time and valuable comment on my thesis. Dr. Barbara Sawicki's extensive knowledge of the photocatalytic technology of TiO_2 brought more insight into this project. Dr. Jerzy A. Sawicki's pleasant discussions regarding the theoretical calculations helped me a lot better understand the project goal. He knew this project and the related preceding work for so long that they can always come up with many constructive suggestions

Many thanks to Dr. Elaine Humphrey for training me on SEM and carbon coater. She extensively helped me by suggesting different image processing techniques, sample preparation techniques. She was so friendly to work with and the most experienced person in this field of imaging of micro and nanoscience at the University of Victoria. And again, thanks to Jonathan Rudge for being the rescuer when I was in trouble while taking SEM images and enriched me with technical knowledge.

Again, I am grateful to Dr. Vahid Moradi for teaching me all the basics and important steps for this project. He guided me and gave m different assignments related to this research and

encouraged me by working by my side. If anything went wrong in my research or in my personal life he was like my brother and suggested a million of the way out.

I would like to give thanks to all my friends I met during my master's program who always supported me and cheered me up whenever I needed positive strength. I would like to mention and thank my lab coworkers in the lab, especially Muniyat Siddiqui Rafa, Subrina Shahid, and Atieh Parisi Couri for all their help. It has truly been a pleasure working with you all.

Very special gratitude goes to my elder brother, Dr. Farid Ahmed. Thank you for your care, unconditional love during all my good and bad times in Canada. You gave me the courage and supported me with all your means to face up all the challenges in life.

Finally, I would like to express my deepest gratitude to my dearest parents. Thank you for your endless love and constant encouragement all the time. Your love is the source of my happiness.

Chapter 1 Introduction

1.1. Motivation

Water is one of the major elements of earth, on which all living creatures depend on to survive. About 71% of the earth's surface is water, but the sources of clean drinking water are decreasing rapidly with urbanization and industrialization. This clean water crisis is believed to be more severe in the upcoming decades. The scarcity of drinkable and uncontaminated water has become a major global environmental issue, even in regions currently considered as water-rich [1]. Water is life, but polluted water is one of the reasons behind mass death. Every year approximately 10-20 million people die because of waterborne and also nonfatal infection is responsible for the death of more than 200 million people [2]. Waterborne disease like Diarrhea has become a major threat to children and about 5000-6000 children die every day in the whole world [3], [4]. Therefore, purification and recycling of industrial and municipal wastewater are necessary.

Nowadays, one of the most advanced and worldwide accepted water treatment techniques is the heterogeneous semiconductor photocatalysis. TiO_2 semiconducting material is mostly used as photocatalyst because of its large bandgap (3.2ev), high chemical stability, non-toxicity, and low-cost [5]. On the other hand, the large bandgap restricts its applications under visible-light illumination, which consists of a wide range of the solar spectrum. To solve this problem, several attempts have been made, one of them is doping a transition metal ion to anatase TiO_2 crystal lattice [6]. Fe is the best suited transitional metal to dope TiO_2 because of the ionic radius of Fe^{3+} (0.69A) which is close to Ti^{4+} (0.745A). Furthermore, the iron ion can act as an electron and hole trap and lowers the bandgap energy into the range of the visible light spectrum. This electron and hole interact with O_2 and OH^- and generate superoxide radical $O_2^{\bullet -}$ and hydroxyl radical $OH^{\bullet}$ respectively. The highly reactive $OH^{\bullet}$ clean the water by reacting with the organic pollutants

present in the water and produce H_2O and CO_2. However, our lab produced Fe-TiO_2 nanocrystals, in the beginning, did not show a promising efficiency in the treatment of model pollutants in water, even though it was considered to be one of the most suitable dopants according to the literature review [7]. The catalytic activity problem was solved by Vahid Moradi using an acid (HCl) treatment to synthesize clean Fe-TiO_2 nanocrystals that removed amorphous contamination layers from the nanocrystal's surface resulting in a boost of its photoactivity from ~20% up to ~100% of 20ppm Methyl Orange (MO) within an hour [8].

This thesis focuses on improving the existing degradation efficiency of Fe doped TiO_2 by working on the details of the photocatalytic crystals syntheses such as increasing the exposed surface area of the crystals by breaking down their agglomerates and securely fusing a large range of crystal sizes onto fiberglass cloth tested in the wastewater reactor resulting in a positive achievement in the degradation of pollutants by reducing the cluster size of the agglomerates. A novel method was also developed to calculate the photo-induced ion current on the coated fiberglass cloth. This research also investigated the best possible way to coat the fiberglass cloth and test their effectiveness against pollutants in water.

1.2. Objective

The following summarizes the objectives in the process of introducing a new idea of a waste-water treatment photoreactor.

- **Investigate the influence of different means of crystal preparation and dip coating techniques for degradation efficiency of Fe-TiO_2** Reduced Crystal cluster size greatly influence the degradation of organic pollutant compared to previous research data. Wet and

dry grinding for a certain period and for several times were done. For further lowering the size of clusters Sonication in alcoholic suspension was performed.

- **Design and develop a prototype photoreactor for water cleaning**. The main goal of this project was to scale up the water cleaning from the laboratory scale of 100 ml to a larger scale of 16 liters. My objective was to design a photoreactor and find a proper way to immobilize the Fe-TiO_2 particles in the reactor system and then finally adjust some parameters of the photoreactor such as light and electrolysis voltage, to enhance the efficiency of pollutant degradation in the water.

1.3. Thesis outline

To better understand this research, the information of previous studies, experiments, and results will be presented divided up into the following chapters.

- Chapter 1 includes a brief introduction that discusses the motivation of this research and provides an idea about the final goal of the research.
- Chapter 2 reviews related fundamental basics of water pollution, pollutant, and briefly explain existing water treatment technologies. Moreover, this chapter discusses how the semiconducting properties of TiO_2 benefit us in water cleaning and also talks about the role of Fe in bandgap engineering of TiO_2 to make the crystals photoactive into the visible range of the light spectrum.
- Chapter 3 discusses the pre-established sol-gel synthesis process and how the multiple mechanical grinding and acid treatment to crystal clusters eventually affect the wastewater cleaning ability. The considerable efforts to enhance photoactivity of the wastewater cleaner will be presented involving different techniques of coating fiberglass cloth with Fe-

TiO_2 crystals. Each of these techniques will be briefly explained in this chapter and Later, there is a description of how the functionalized fiberglass cloths were used in the prototype photoreactors.

- Chapter 4 presents a summary of all the experimental results used to characterize selected degradation parameters. It also explains how a small change of a parameter of the photoreactor influences the degradation efficiency.
- Chapter 5 will briefly discuss experimental results and their achievements.
- Chapter 6 will share the possible future steps to modify the present photoreactor and will give some other possibilities of using this technology in various environments and in everyday life.

Chapter 2 Literature Review

2.1. Water Pollution

The presence of solid, liquid, or gaseous contaminants in water may alter the quality of the water. If it has an adverse effect on any living thing that drinks or lives on it, it is called water pollution. In general, wastewater contains high levels of organic material, numerous pathogenic microorganisms, as well as nutrients and highly toxic compounds. These pollutants cause environmental and health hazards and, consequently, measures should be taken before releasing this contaminated water into nature. The ultimate aim of wastewater treatment is the protection of the environment in a manner commensurate with public health and socioeconomic concerns [9].

2.1.1. Water pollutants

Before discussing water treatment and reclamation, the qualitative and quantitative nature of the pollutants in the water should be one's first concern. Many pollutants are present in wastewater, but toxicity is only observed beyond a certain limit called the permissible limit. The water pollutants may be categorized as:

Inorganic: The most common inorganic water pollutants are heavy metals, which are highly toxic and carcinogenic in nature such as nitrates, sulfates, phosphates, fluorides, chlorides, and oxalates, etc.

Organic: The toxic organic pollutants are from pesticides which include insecticides, herbicides, fungicides; polynuclear hydrocarbons (PAHs), phenols, methyl orange, polychlorinated biphenyls, halogenated aromatic hydrocarbons, formaldehyde, polybrominated biphenyls, biphenyls, detergents, oils, greases, etc. In addition to these, normal hydrocarbons, alcohols, aldehydes, ketones, proteins, lignin, pharmaceuticals, etc. are also found in wastewater.

Biological: Different types of microbes growing in wastewater may be responsible for different types of diseases. The harmful microbes include bacteria, fungi, algae, plankton, amoeba, viruses, and other worms. These water pollutants remain either in solvated, colloidal, or in the suspended form [10].

2.1.2. Model pollutants of this research

Methyl Orange (MO): Methyl Orange is an organic photoactive azo dye, well known for its excellent optical switching properties, good chemical stabilities and high solution process abilities [11][12][13][14]. Moreover, the use of organic dyes is increasing with the growing textile industries and hence pollution in water goes up due to dyestuff [15]. Textile industries consume a huge quantity of water for the dying process and generate a significant amount of effluent pollutants. A survey reveals that about 280,000 t of textile dyes are discharged as industrial effluents every year worldwide [16]. This azo dye contains a characteristic azo group (–N=N–) in its chemical structure and makes up about 70% of all dyestuff by weight worldwide[17]. For being the largest colorant group in textile industries, they are also responsible for major contamination of water [18]. Untreated discharge of azo textile die in an aquatic system causes mass destruction for any living being by toxifying the water, reducing oxygen concentration. [19]. Therefore, one of the azo group representative Methyl Orange (MO) was chosen for this research. The chemical structure of methyl orange is shown in Figure 2.3 [14]:

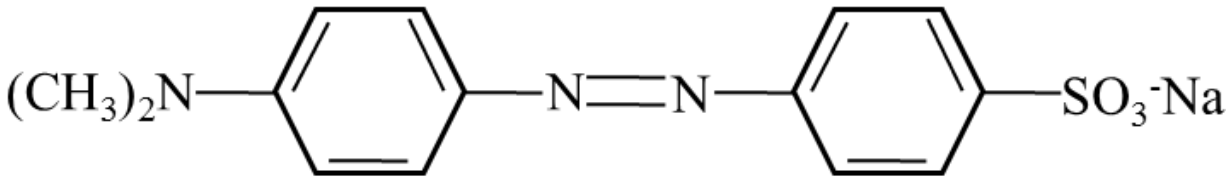

Figure 2.1 Chemical structure of Methyl Orange

Phenol: the second model pollutant used in this research was phenol which is a colorless crystalline solid containing benzene ring in its chemical structure. It is a colorless toxic chemical with a special odor, soluble both in water and organic solvents.

The phenolic compound has a versatile use in domestic, agricultural, and industrial purposes. They can be used as the component of dyes, polymers organic substance, and drugs. Their presence in the environment could happen through numerous pesticides, industrial waste, and municipal sewage. [20]. The presence of phenol in water is a prime concern because of its chemical stability, water solubility, and environmental mobility [21]. Phenol's toxic behavior is not yet fully specified but known as harmful eco toxins because of its hydrophobicity and generation of organic radicles. [20]. The damaging effect of phenol in the marine environment is huge [22] and that is why this is an ideal pollutant representative in this project. The chemical structure of phenol can be represented in figure 2.2 [23].

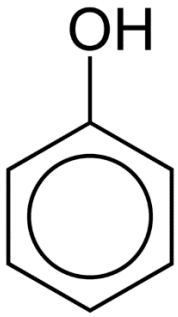

Figure 2.2 The chemical structure of Phenol.

2.2. Wastewater treatment technologies

There are several technologies for water treatment, but scientists are still doing their research to find out the most convenient, inexpensive, and environmentally friendly technologies. Water treatment technologies are used for three purposes i.e. water source reduction, wastewater

treatment, and recycling. Water treatment and recycling technologies can be classified under the following three main classes (figure 2.3) [10].

- Primary water treatment technologies
- Secondary water treatment technologies
- Tertiary water treatment technologies

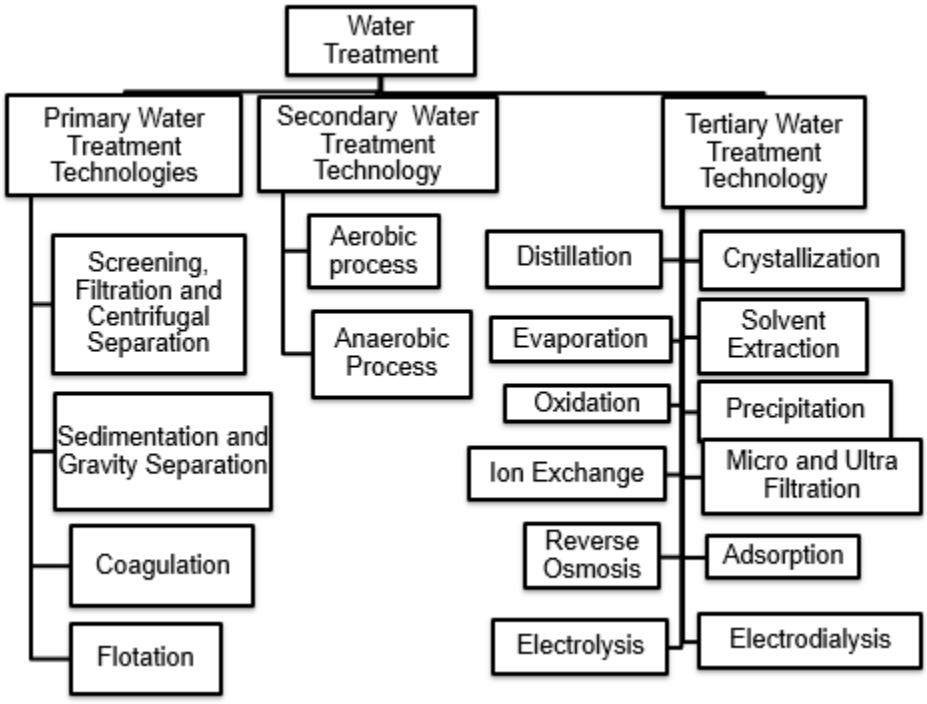

Figure 2.3 Illustration of the classification of chemical treatment and water recycling technologies [10].

2.2.1. Primary water treatment technologies

In primary water treatment technology, water is treated using screening, filtration, centrifugation, sedimentation, coagulation, gravity, and flotation methods. Primary water treatment technologies are for highly contaminated water, mostly to get rid of solid bodies from the water. These methods are shortly discussed below

Screening, filtration and centrifugal separation: The main purpose of **screening** is to remove the solid waste present in the wastewater, and it is used for the removal of pieces of cloth, paper, wood, cork, hair, fiber, kitchen refuse, fecal solids, etc. Normally, a setup with a pore size of about 0.1 to 0.5 mm is used for this purpose. It is used for the removal of suspended solids, greases, oils, bacteria, etc. **Centrifugal** separation is used to remove suspended non-colloidal solids (size up to 1 mm) [24].

Sedimentation and gravity separation: Different kinds of tanks are used to separate the suspended solids, grits, and slits by allowing the wastewater undistributed or semi-distributed for the different time intervals. The suspended solids settle under the influence of gravity [25].

Coagulation: All the suspended solids cannot be separated by the sedimentation and gravity separation method and, hence, non-settleable solids are allowed to settle by the addition of certain chemicals, this process is called as coagulation [26].

Flotation: In this process the suspended solids, oils, greases, biological solids, etc. are removed by adhering them with either air or gas in the flotation process [27].

2.2.2. Secondary water treatment technologies

Secondary water treatment technology uses biological processes to eliminate soluble and insoluble contaminants by microbes. This process includes the aerobic and anaerobic digestion of wastewater [28].

Aerobic processes: In the aerobic process aerobic and facultative bacteria decompose biodegradable organic matters in the presence of air or oxygen which is dissolved in wastewater. The extent of the process depends on the availability of oxygen, retention time, temperature, and

the biological activities of the bacteria. A simplified form of aerobic decomposition is given by the following equation [29].

$$\text{Organic matter} + O_2 + \text{Bacteria} \longrightarrow CO_2 + H_2O + \text{Bacteria} + \text{Byproducts} \text{ ----------2.1}$$

Anaerobic process: If free dissolved oxygen is not available in the wastewater then anaerobic decomposition, called putrefaction, occurs. The anaerobic process is represented by the following equation [30], [31].

$$\text{Organic matter} + CO_2 + \text{Bacteria} \longrightarrow CO_2 + CH_4 + \text{Bacteria} + \text{Byproducts} \text{ -----2.2}$$

2.2.3. Tertiary water treatment technologies

Among the water treatment technologies tertiary water treatment technologies are the most important because these are used to obtain safe water for human consumption. Some of the techniques are distillation, crystallization, evaporation, solvent extraction, oxidation, Advanced oxidation process, coagulation, precipitation, electrolysis, electrodialysis, ion exchange, reverse osmosis, and adsorption. These methods are shortly described below.

2.3. Advanced oxidation processes

Advanced Oxidation Processes (AOPs) are a tertiary water treatment process that has gained popularity for the post-treatment of industrial effluent. When a single oxidation process is not sufficient for the total decomposition of organic pollutants present in wastewater, then AOPs are applied. AOPs are processes involving the simultaneous use of more than one oxidation process and involve the accelerated production of the highly reactive hydroxyl free radical [10]. During AOPs, organic compounds are generally decomposed or transformed into biodegradable form and which prevents secondary loading of a contaminant in the environment. Therefore, AOPs are considered as “clean technologies” [32].

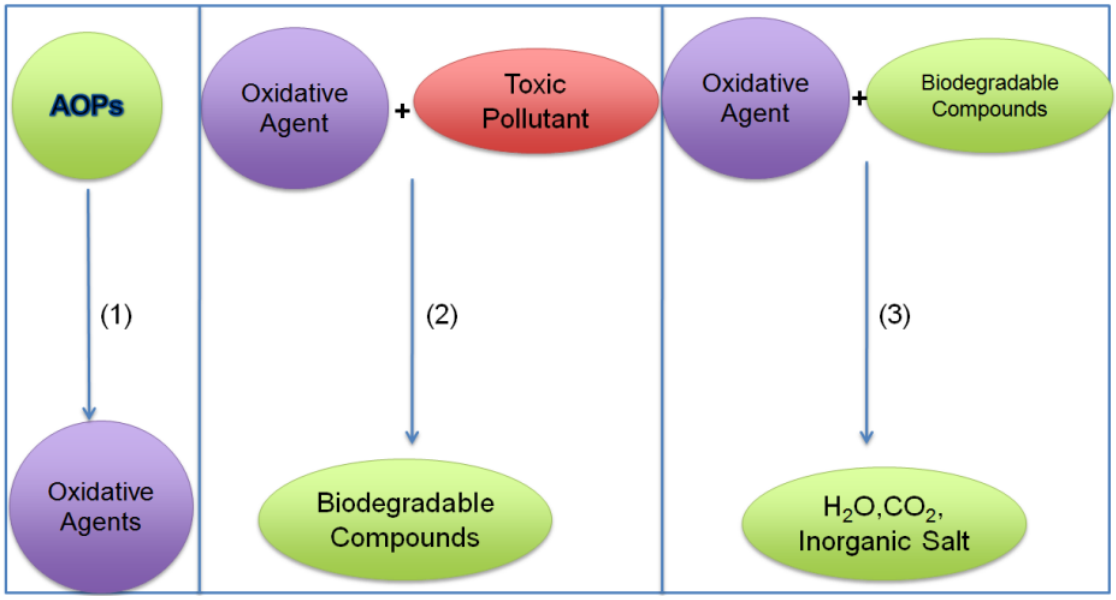

Figure 2.4 Simplified steps of Advanced Oxidation Processes.

According to the accepted theory, AOPs are processes involving the simultaneous use of more than one oxidation process and involve the accelerated production of the highly reactive hydroxyl free radical •OH. Hydroxyl radicals are non-selective species and have a high electrochemical oxidation potential of E_0=2.80 eV, which makes them a powerful oxidant to decompose organic pollutants that cannot be destroyed by other conventional oxidants (oxygen, ozone, and chlorine) [33]. The oxidation potential values of different oxidants are listed in Table 2.1 and show that the •OH radicals are extremely powerful oxidants.

Table 2.1 Standard electrochemical reduction potentials of some common oxidants [34]

oxidant	**Half-cell reaction**	**Oxidation potential (V)**
OH (hydroxyl radical)	$^{\bullet}OH + H^+ + e^- \rightarrow H_2O$	2.80
O_3 (ozone)	$O_3(g) + H^+ + 2e^- \rightarrow O_2(g) + H_2O$	2.07
H_2O_2 (hydrogen peroxide)	$H_2O_2 + 2H^+ + 2e^- \rightarrow 2H_2O$	1.77

HOCl (hypochlorous acid)	$2HOCl + 2H^+ + 2e^- \rightarrow Cl_2 + 2H_2O$	1.49
Cl_2 (chloride)	$Cl_2(g) + 2e^- \rightarrow 2Cl^-$	1.36

The $^{\bullet}OH$ radicals can subsequently, when sufficient contact time is available, oxidize organic species into CO_2 and H_2O [34].

AOPs can be divided into two broad classes, homogeneous and heterogeneous based on the reactive phase as shown in figure 2.5.

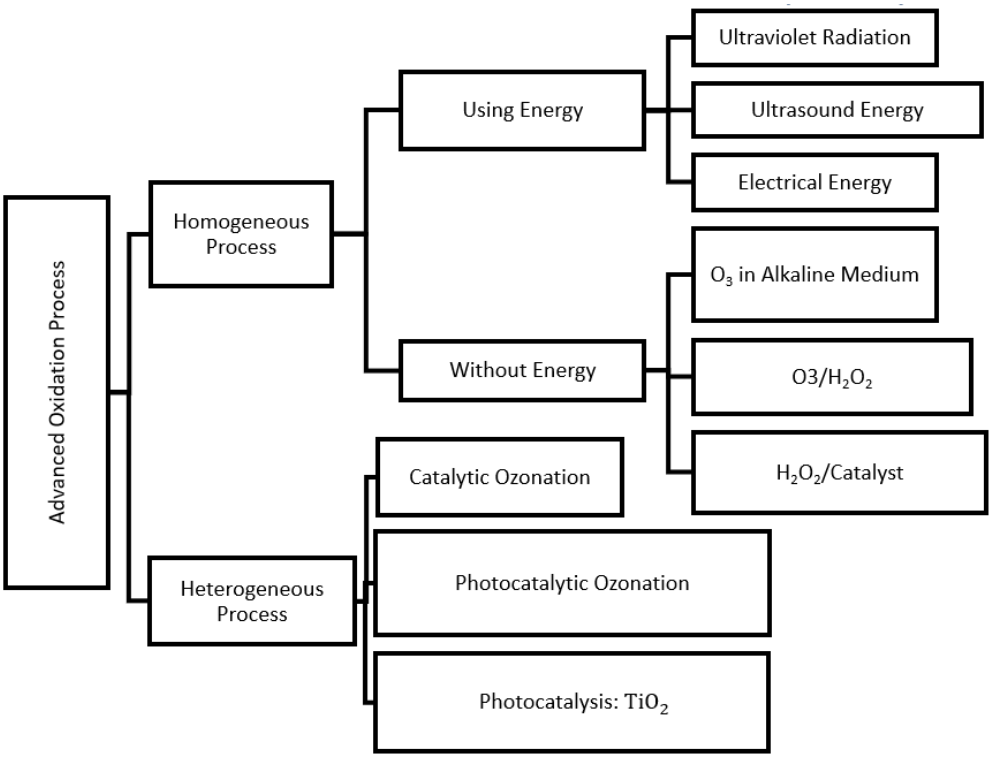

Figure 2.5 Classification of AOP [33].

2.3.1. Homogeneous photo-oxidation

In this process, the precursor remains in an undissolved form in water and generates free radicals that react with the dissolved substances in the aqueous phase [35].

Examples: Fenton based process (Fenton, Fenton like Sono-Fenton, Photo-Fenton, Electro-Fenton, Sono-electro-Fenton, Photo-electro-Fenton, Sono-photo-Fenton) and O_3 based processes (O_3, O_3 + UV) and H_2O_2 based processes (H_2O_2 + UV) and their combination can be emphasized [33].

2.3.2. Heterogeneous photo-oxidation

In this process, the solid precursor generates free radicals at the solid-water interface, and the oxidation reaction takes place at the solid-water interfacial region with the adsorbed pollutant substance.

Examples: Photocatalysis, catalytic wet peroxide oxidation, catalytic ozonation, etc. are heterogeneous conventional AOPs [33].

2.4. Photocatalysis

In recent days heterogeneous photocatalysis has become a hot topic and widely studied because of its efficient energy-saving and economy in water and air purification. In the last decade, the number of scientific papers containing word photocatalysis or photocatalyst in the title exceeds 9000. Photocatalysis is a chemical reaction that takes place on the surface of semiconducting material in the presence of photon or light. Photocatalysis is usually referred to as photocatalytic activity. There is no chemical change that takes place during and after the photocatalytic reaction on the photocatalyst. The photocatalytic process in water can be divided into five steps:

- Transfer of reactants in water to the surface of photocatalysts,
- Adsorption of reactants on the surface,
- Photonic activation of the surface of photocatalyst and reaction in the adsorbed phase,
- Desorption of reaction products,
- Elimination of reaction products from the interface region.

2.5. TiO_2 as photocatalyst

Titanium dioxide (TiO_2), CI 77891, also known as titanium (IV) oxide or Titania was discovered in the year 1821 and is reported to be one amongst the top 20 inorganic chemicals of industrial importance [36]. TiO_2 is a semiconductor, it has an excellent charge transportability making it a very good candidate as a photocatalyst [37][37]. Moreover, it is widely used as a pigment in paints, coatings, sunscreens, ointments, and toothpaste because of its brightness having a very high refractive index. When it is used as a pigment, it is known as “Titanium White” and “Pigment White 6”. TiO_2 is generally sourced from a variety of ores such as ilmenite, rutile, and anatase. The two most common crystalline forms of TiO_2 namely, anatase and rutile, are produced from titanium mineral concentrates either by the older sulfate or a newer chloride process [38].

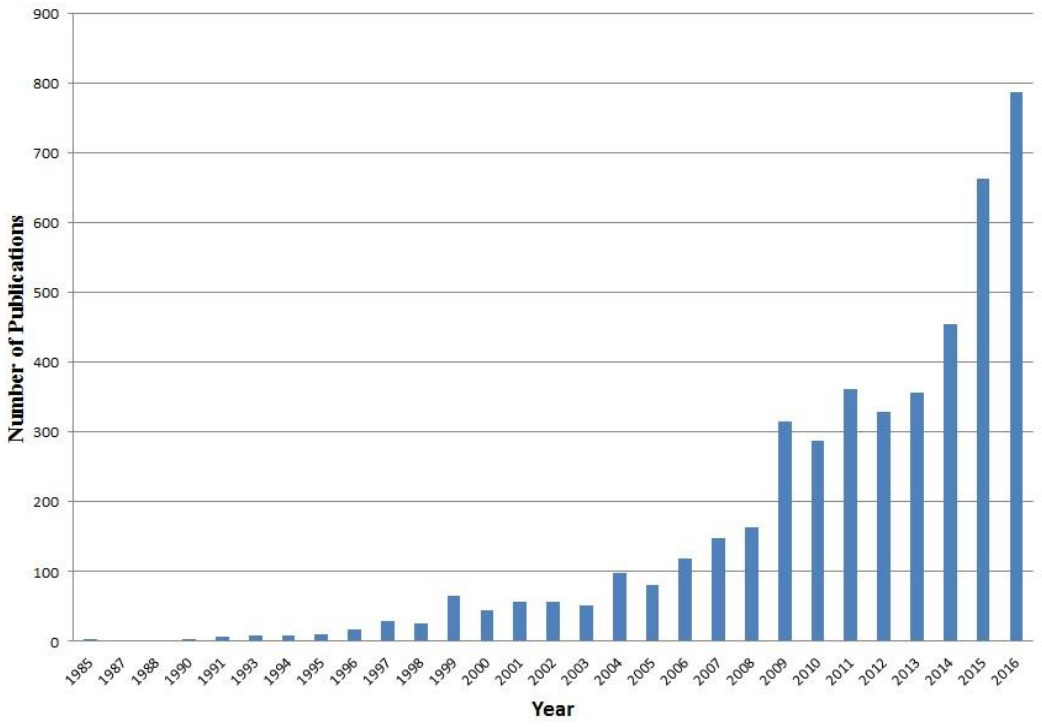

Figure 2.6 Number of publications registered on the keywords ”photocatalysis” and ”water treatment” in the Scopus database from 1985 to 2016, retrieved from Scopus.com (2017).

The photocatalytic activity of TiO_2 was first discovered by Fujishima and Honda in 1972. They found that water could be photocatalytically oxidized and reduced at the same time. This finding opened a new door to treat wastewater. Since then a tremendous amount of research has been going on and till now scientists are working to improve and enhance the photocatalytic activity of Titania [39].

2.5.1. Structure & properties of TiO_2

Titanium dioxide commonly exists in three common polymorphs such as anatase, rutile, and brookite. Their crystal structures are shown in figure 2.7.

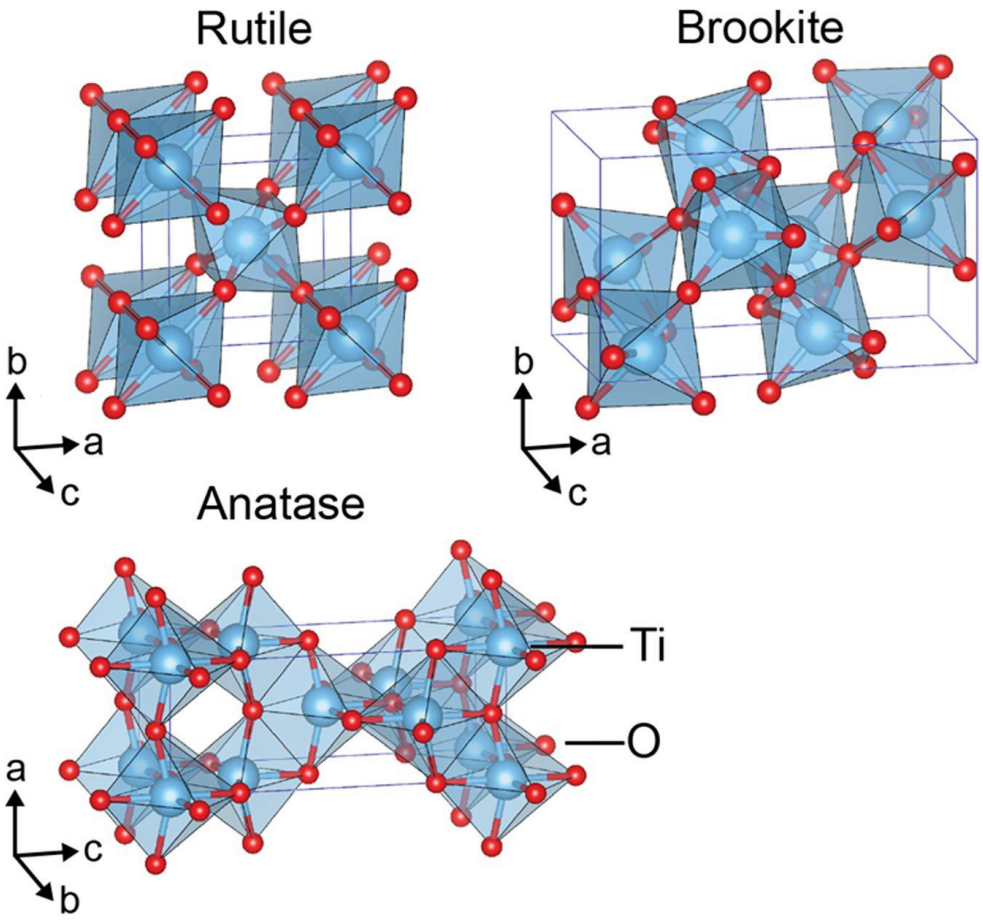

Figure 2.7 Crystal structures of three TiO2 polymorph [40].

among the three polymorphs, anatase and rutile have tetragonal crystal structure where each Ti atom is coordinated with six O, and each O is coordinated with three Ti. Each Anatase and Rutile structure is slightly distorted where four Ti-O bonds are identical and longer than the other two identical Ti-O bonds. Again, Brookite has an orthorhombic crystal structure and all of its Ti-O bonds are different in length. [24], [40]. Some of the characteristic properties of anatase, rutile, and Brookite are listed in table 2.2.

Table 2.2 Properties of anatase, rutile and brookite polymorph of Titania

Properties	**Anatase**	**Rutile**	**Brookite**
Crystal structure	Tetragonal	Tetragonal	Orthorhombic
Lattice constant (Å)	a = 3.784 c = 9.515	a = 4.5936 c = 2.9587	a = 9.184 b = 5.447 c =5.154
Molecule cell	2	2	4
Volume ($Å^3$)	34.061	31.2160	32.172
Density (g/cm)	3.79	4.13	3.99
O-Ti-O bond angle	77.7° 92.6°	81.2° 90.0°	77° - 105°

2.4.1. The basic principle of photocatalysis (UV \TiO_2)

The photocatalysis process depends on the electronic structure of semiconductors (TiO_2). The electronic structure of a semiconductor consists of a valance band (VB) and a conduction band (CB). The energy difference between these two levels is referred to as the bandgap energy (E_g). The bandgap energy of anatase TiO_2 is 3.2 eV. Therefore to activate the photocatalytic activity of anatase UV light of $\lambda \leq 387$ nm is required to illuminate [35]. When light irradiates the TiO_2, it

absorbs the energy equal to or greater than its bandgap energy, electron-hole pair form, positively charged holes (h^+) at the valance band (VB) and negatively charged electrons (e^-) at conduction band. If organic pollutants of lower oxidation potential are absorbed on the surface of the photocatalyst, the created charge carriers in the CB and VB reduce and oxidize the pollutants respectively, However, recombination of these charge carriers can occur (Figure 2.8) causing no chemical reaction [33].

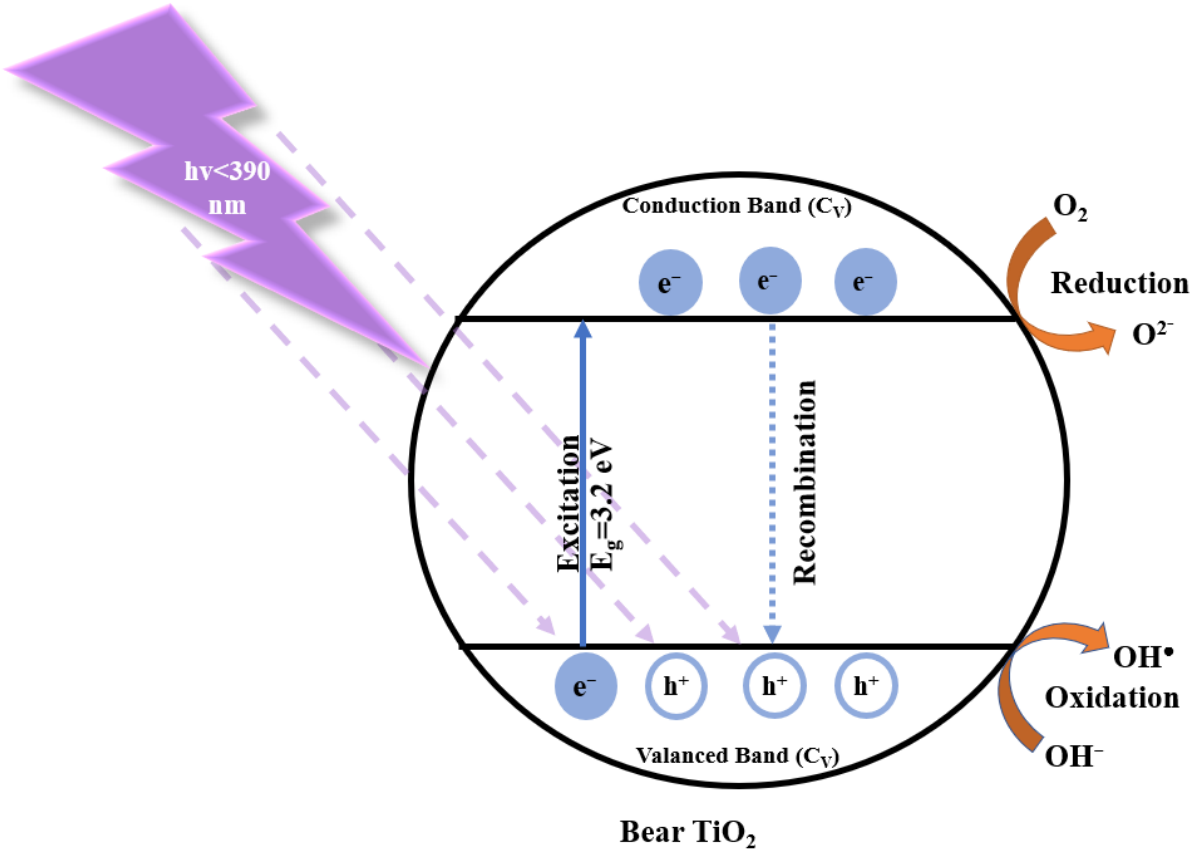

Figure 2.8 Schematic reaction mechanism of TiO_2 photocatalyst with UV light and the production of holes in the VB by the excitation of electrons to the CB [34].

Advantages of using photocatalyst in water treatment

In photocatalytic water treatment, semiconductors are activated by the consumption of photons from light to produce electron-hole pair that initiates the oxidation-reduction reactions.

The advantages of using this process are summarized by Malato et al. as follows:

- The process takes place at normal pressure and at ambient temperature.
- The oxygen demand for the electron capture reaction can be directly obtained from the atmosphere.
- The catalyst is inexpensive, safe, and, in principle, can be reused.
- The catalyst can be immobilized on different types of substrates.
- The solar light can activate and excite the catalyst.

Among different semiconductors, TiO_2 is the most used photocatalyst since it is affordable, environmentally friendly, non-toxic, chemically resistant, and reusable [41].

2.5.1. Why TiO_2 applications are limited

Among various photocatalyst TiO_2 is the most commonly used and believed to be an ideal photocatalyst because of the following reasons:

- TiO_2 has the ability to completely mineralize the target pollutants.
- TiO_2 is cheap and abundant.
- Photostable in solution.
- High efficiency and
- Nontoxicity

Limitations of TiO_2 as photocatalyst

However, it has some disadvantages that limit its photoactivity. Some of the downsides are as follows:

- The relatively high value of the bandgap, around 3.2 eV, limits its use to UV light.
- TiO_2 has a dispersion in the water which causes difficulties in sedimentation, and
- Sensitivity to the electrons and holes recombination, which decreases its photocatalytic activity.

To solve the problems researchers are trying to improve the separation between the free carrier, increasing the adsorption abilities of the photocatalyst surface, or by adding impurity on photocatalyst to improve photocatalytic activity [42]. Electron hole recombination limits the quantum yield achievable. Transitional metal cations doping in Titania is the most effective way to enhance photocatalytic properties by inhibiting the recombination of the charges [43], [44], and [1].

2.5.2. Modification of TiO_2

An unmodified TiO_2 nanocrystal shows photocatalytic activity only in the ultraviolet spectrum (~300-400 nm) which accounts for only 4% while visible light (~400-700 nm) accounts for 43% of the solar light. Hence, to improve the photocatalytic activity of TiO_2 towards the visible area (~400-700 nm) different modification methods such as coating organic dyes, doping with metal ions, heavy metal precipitation, size modification, system modification and so on can be taken (figure 2.9).

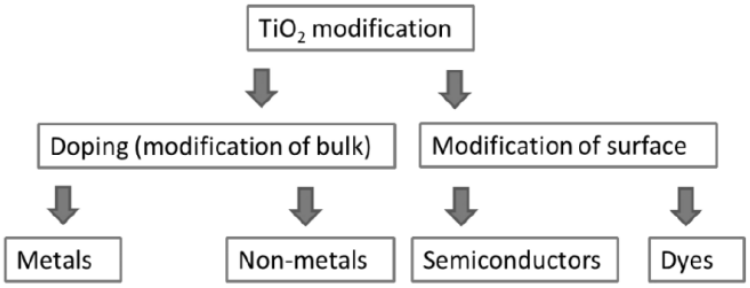

Figure 2.9 Modification pathways of TiO_2.

2.5.3. Doping TiO_2 with metals

TiO_2 semiconductor can be photocatalytically activated in the visible light spectrum by inserting a metal impurity into the TiO_2 lattice by different methods [45].

- One way of modifying the bandgap of TiO_2 photocatalyst is the molecular combination of metal oxide in the TiO_2 lattice.
- Novel metal deposition on TiO_2 crystallites.
- Impregnating TiO_2 with metal salt by evaporation
- Introducing transitional metal into the TiO_2 precursor solution.

2.5.4. Fe doped TiO_2

For the water treatment, there are different preparation methods of Fe doped TiO_2 to maintain good control of particle size and morphology in the nano-scale range. Fe^{3+} is an interesting dopant in TiO_2 because it has the ability to act as a shallow trap for the electron and holes in TiO_2 lattice and enhance the recombination life time[46], [47]. Among the transitional metals, iron is the most appropriate dopant in TiO_2 because of its relative radius size. The radius of Fe^{3+} (0.69A) is similar to that of Ti^{4+} (0.745A), so Fe^{3+} can be easily introduced into the crystal structure of TiO_2. Again the energy level of Fe^{2+} / Fe^{3+} is close to that of Ti^{3+} / Ti^{4+} which favors the photogenerated electron and hole to remain separate [48], [1].

2.5.5. System modification

In general, for the sake of large surface area, TiO_2 nanoparticles were used in a slurry system. The recycling in this slurry system led to mass loss and may cause secondary pollution. Therefore, to get rid of this problem, researchers have been trying different methods. TiO_2 nanoparticles could be immobilized on a different solid substrate, like alumina, glass slides, steel plate, polymer, and so on.

- In Gelover et al.'s study, TiO_2 and glass pieces were connected together to avoid the post-separation process [49].
- Kieda and Tokuhisa [50] uniformly deposited TiO_2 nanoparticles on metal substrates electrolytically.
- Zeng et al. [51] prepared a kind of portable composite film by fixing TiO_2 onto cellulose via the sol-gel method and these films could remove phenol at a high rate.
- Lei et al. [52] immobilized TiO_2 in a PVA matrix by forming a Ti-O-C chemical bond through the solution-casting and heat-treatment method.

2.6. Mechanism of photocatalytic processes in Fe-doped TiO_2

Iron doping in Titania plays a great role in the improvement of the photocatalytic activity by inhibiting the recombination of the photogenerated electron and hole. According to most of the studies, there are two types of configuration energy levels. One is the oxidation level (Fe^{4+} / Fe^{3+}), which lies above the valance band energy level and the other is the reduction level (Fe^{3+}/Fe^{2+}), which is below the conduction band of pure TiO_2. As the light source illuminates the TiO_2 surface, one electron migrates from TiO_2 to Fe^{3+} and produces Fe^{2+} (Equation 2.3). Due to the loss of the d^5 electron, Fe^{2+} has a tendency to return to its most stable form Fe^{3+}. Consequently, Fe^{2+} ion oxidized to Fe^{3+} ions, transferring one electron to absorbed O_2 to form highly reactive superoxide O_2^- anions (Equation 2.4). At the same time, Fe^{3+} may act as a hole trap (Equation 2.5). Again, as

the Fe^{3+} / Fe^{4+} lies above the valance band energy level of TiO_2 so that Fe^{4+} could be reduced to Fe^{3+} by gaining one electron from OH^- ion leaving behind a hydroxyl radical, $OH^{\bullet}$ (Equation 2.6).The hydroxyl radical produced on the surface of the TiO_2 is a great oxidizing agent which can oxidize organic pollutants [5]. The entire process is briefly shown in figure 2.10.

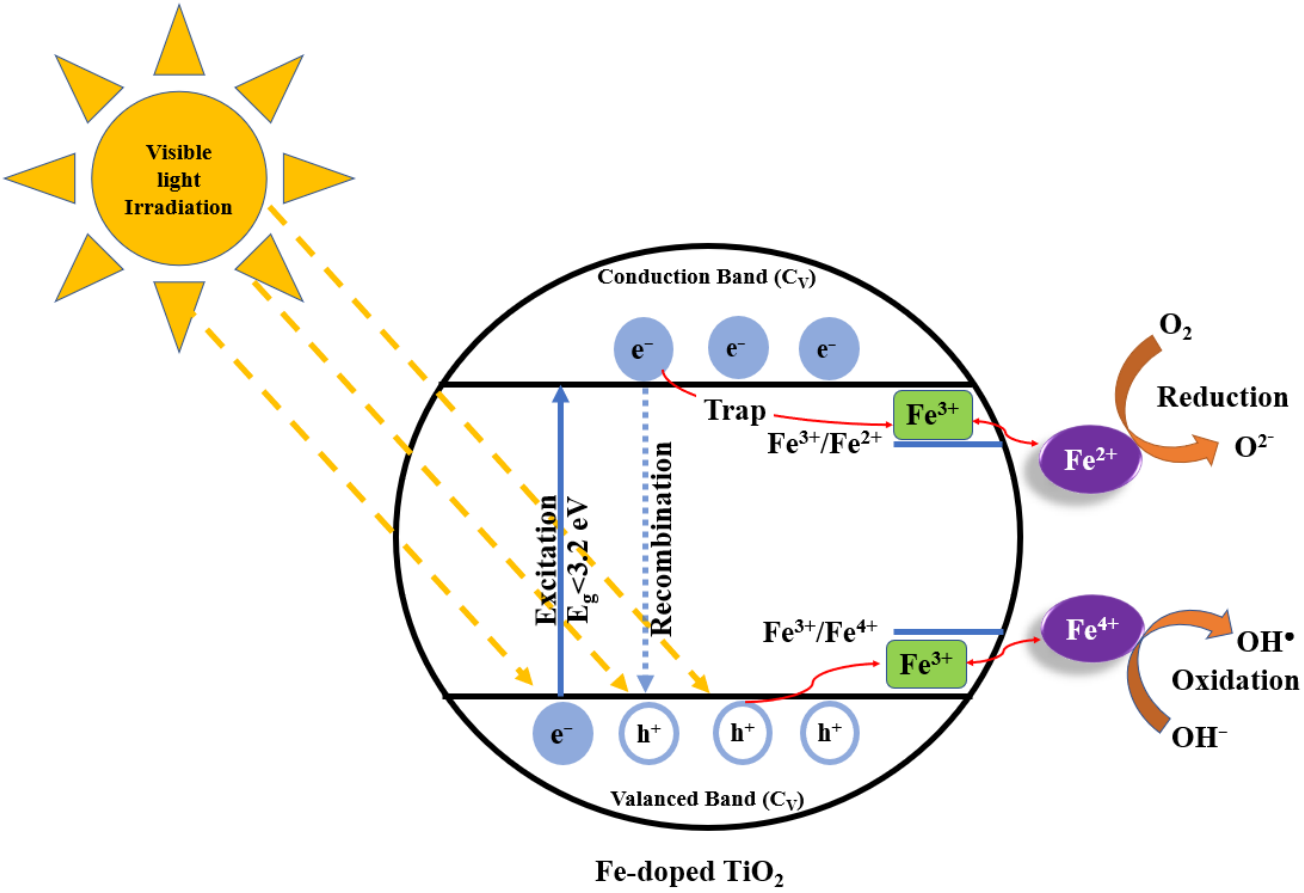

Figure 2.10 Schematic band diagram for the transport of charge carriers from excited TiO_2 NPs to the different energy levels of Fe^{3+}ions [5].

$$Fe^{3+} + e^- \longrightarrow Fe^{2+} \quad \text{.....2.3}$$

$$Fe^{2+}O_{2(ads)} \longrightarrow Fe^{3+} + O_2^- \quad \text{.....2.4}$$

$$Fe^{3+} + h^+ \longrightarrow Fe^{4+} \quad \text{.....2.5}$$

$$Fe^{4+} + OH^{-} \longrightarrow Fe^{3+} + OH^{\bullet} \text{.....2.6}$$

The photocatalytic activity can be measured in a very simple manner by measuring the degradation of pollutants in water. In this technique, a known concentrated pollutant solution is made and concentration of before and after treatment is measured. A simple equation is used to measure percent degradation (*X%)* as follows:

$$X\% = \frac{Co - Cc}{Co} \times 100 \text{.....2.7}$$

Where, C_0 and C_c are the initial and final concentrations of the pollutant, respectively. According to the Langmuir-Henshelwood model the kinetics of the heterogeneous photocatalytic degradation usually follows the equation given below:

$$r = \frac{dc}{dt} = \frac{kKC}{1+KC} \text{.....2.8}$$

where *r, C, t, k, and K* represent the rate of the degradation reaction, the concentration of the pollutant, reaction time, the rate constant of the reaction, and *K* is the absorption coefficient of the pollutant respectively. At extremely low concentration of the pollutant, the above equation can be simplified to:

$$ln\frac{Co}{C} = kKt = Kappt \text{.....2.9}$$

where *Kapp* is the apparent first-order rate constant. The rate constant of a first-order reaction can be obtained by plotting lnC_0/C vs *t* [53].

2.6. Electrolysis:

Electrolysis or electrochemical action is a process of decomposition of a liquid by means of external electric current to its fundamental chemical forms [54]. A fundamental electrolysis cell consists of an anode, a cathode, a power supply, and an electrolyte as shown in Fig (2.11). An

external source of direct current (DC) is connected to the two ends of the cell to maintain balanced electricity and to keep electron flow from the negative terminal (anode) of the source to the positive cathode. When electrons reach the cathode, hydrogen ions consume them and are turned into hydrogen. Again, to keep the electrical charge-balanced in an electrolyte solution, hydroxide ions move towards the positive end of the electrolytic cell through electrolyte solution and give away electrons at the positive electrode (cathode). These electrons then travel through the cathode toward the positive end of the DC source (figure 2.11) [55].

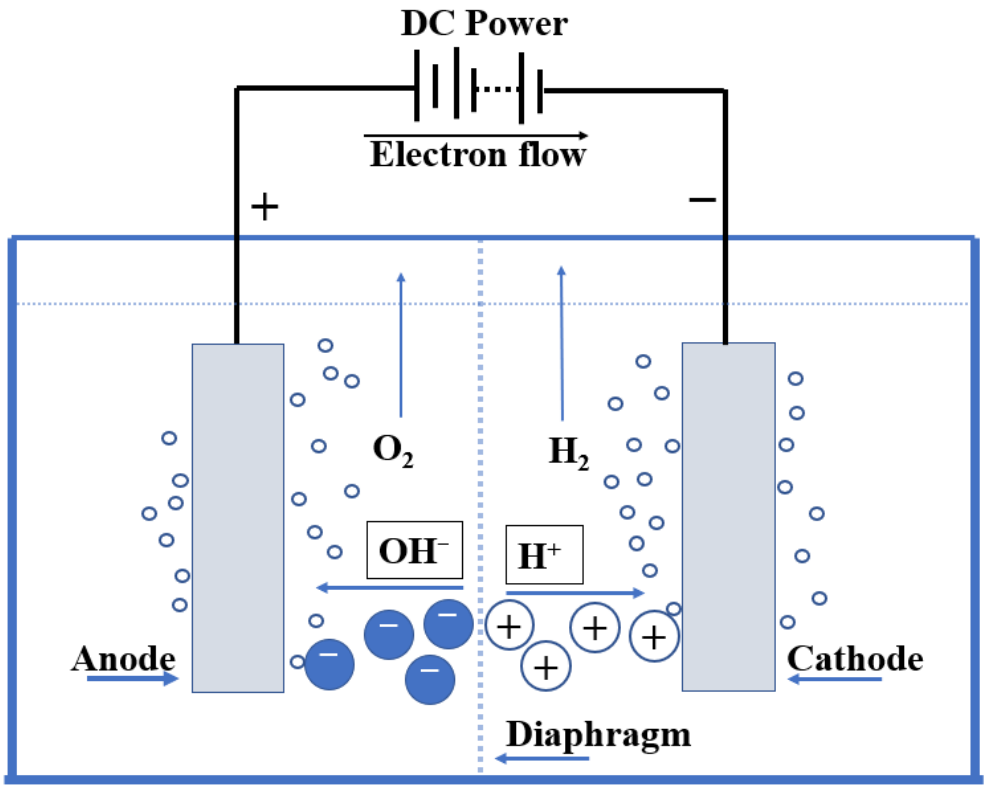

Figure 2.11 A schematic structure of a basic electrolysis system.

The half-reaction occurring in water electrolysis can be represented as follows:

$$\text{Anode (+ve): } 6H_2O(l) \longrightarrow O_2(g) + 4H_3O^+(aq) + 4e^- \text{ (to anode)} \quad \ldots..2.10$$

$$\text{Cathode (-ve): } 4e^- \text{ (from cathode)} + 4H_2O(l) \longrightarrow 2H_2(g) + 4HO^-(aq) \quad \ldots.2.11$$

Overall: $2H_2O(l) \longrightarrow 2H_2(g) + O_2(g)$…….2.12

Where (*l*), (*g*) and (*aq*) represents the states of material, such as liquid, gas, and the aqueous solution respectively [56]. During the electrolysis process of water, a different pH can be observed in the vicinity of the electrodes due to increased concentration of cations and anions on the cathode and anode respectively. If a suitable membrane separates the cathode and anode, then there will be a rise in the concentration of H_3O^+ in anolyte and OH^- in the catholyte and hence increase respective conductivity compared to free mixing of electrolyte in between the electrodes [57].

2.6.1. ˙OH production pathways

In the water electrolysis process, the nature of the dissociation of water could be complex depending on the applied voltage. When the applied voltage is greater than required, side reactions may occur to form some constituent molecules, ions, and radicles in the electrolyte. At low overpotential, the concentration O_2 is high and few O_3 (Ozone) may be present in the electrolyte but with an increase of voltage, O_3 molecule increases. The following ions, molecules, and radicals could be present in the electrolysis cell relying on the electrode material, pH, and applied voltage [58].

Table 2.3 list of molecules, ions, and radicles in anolyte and catholyte

Anolyte (at pH~3.5)	**Catholyte (at pH~10.5)**
$O_2(g)$, $O_2(aq)$, O_3(g), $O_3(aq)$, H_2O_2, H^+, $^{\bullet}OH$, $O_2^{\bullet}$, $HO_2^{\bullet}$	$H_2(g)$, $H_2(aq)$, OH^-, H^-, $H^{\bullet}$, $O_2^{\bullet-}$, $e^-(aq)$, HO_2^-

Ozone in water within a few minutes decomposes to give rise to several strong oxidants including hydroxyl radicals ($^{\bullet}OH$) and superoxide ($O_2^{\bullet-}$) through the following reaction given below [59].

$$2O_3 \longrightarrow 3O_2 \quad \text{2.13}$$

$$O_3 + OH^- \longrightarrow HO_2^- + O_2 \quad \text{2.14}$$

$$O_3 + HO_2^- \longrightarrow {}^{\bullet}OH + O_2^{\bullet -} + O_2 \quad \text{2.15}$$

Again, dissociative recombination of H_3O^+ with an electron plays a vital role to generate hydroxyl radicals in the following manner [60][61].

$$H_3O^+ + e^- \longrightarrow {}^{\bullet}OH + H_2 \quad \text{2.16}$$

$$H_3O^+ + e^- \longrightarrow {}^{\bullet}OH + {}^{\bullet}H + {}^{\bullet}H \quad \text{2.17}$$

2.7. Surface plasmon resonance (SPR)

Surface plasmon resonance (SPR) is an electromagnetic phenomenon of novel metal (normally for gold and silver) that occurs on the metal-dielectric interface (e.g. a metal sheet in the air). Depending on the thickness of the molecular metal layer, when a light beam strikes the surface with a particular angle, the SPR phenomenon results in a graded reduction in the intensity of the reflected light [62].

2.7.1. Particle plasmon

When a light beam irradiates the metallic nanoparticles (where the wavelength of light is higher than the spatial dimension of the metal nanoparticles), the oscillating electric cloud of the nanoparticle gets distorted from its original positions by the influence of the electromagnetic wave of the light. From the distortion of the electron cloud, a restoring force arises because of the coulombic attraction of electrons and nuclei and thus causes plasmonic oscillation, see Figure 2.12 This is how a metallic nanoparticle acts like an oscillator and the oscillation behavior depends on the density of electrons, the effective electron mass, and the size and shape of the charge

distribution. The corresponding resonance behavior determines the optical properties such as the color we observe [63][64].

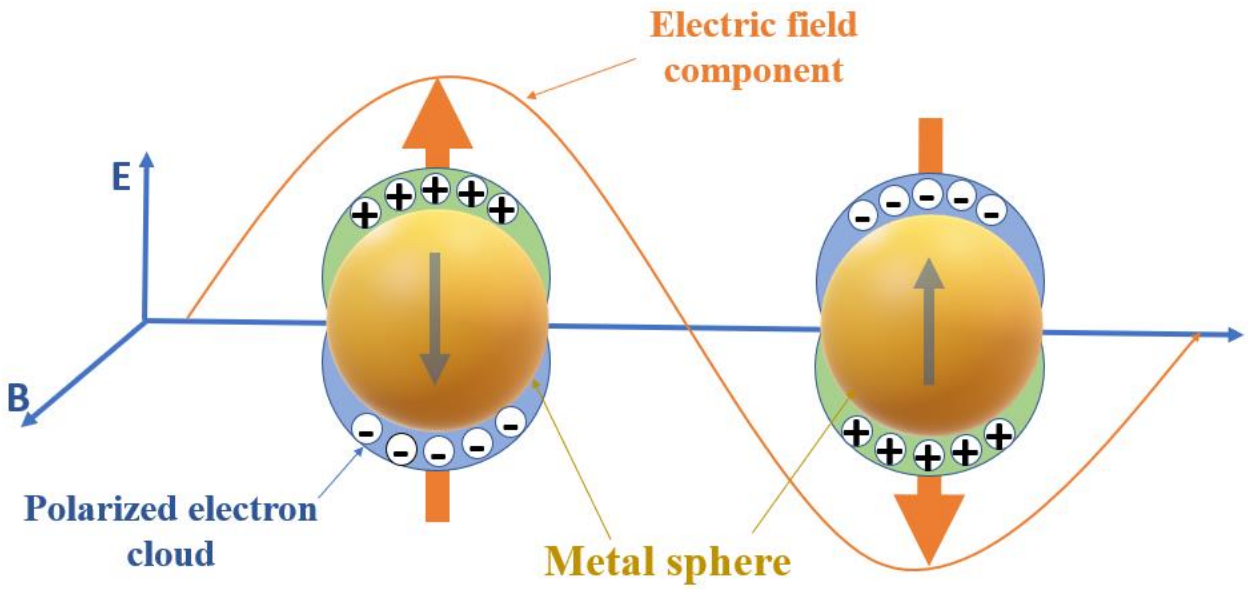

Figure 2.12 Schematic excitation of particle plasmons through the polarization of metallic nanoparticles.

Chapter 3 Synthesis of Fe doped TiO2

This chapter explains the synthesis steps of Fe doped TiO_2 crystals and its coating methods on fiberglass cloth. This chapter also illustrates the construction of a photoreactor and the installation of coated fiberglass in the photoreactor.

There are many crystals synthesis processes being used for Fe doped TiO_2 nanocrystals, including sol-gel, chemical vapor deposition [65], hydrothermal, direct oxidation method [66], ultrasonic irradiation [67], solvothermal [68]. The sol-gel method is widely used because of its simplicity and low cost even though the catalyst synthesized can be highly pure [69].

3.1. The sol-gel technique for Fe doped TiO_2 synthesis

The Fe doped TiO2 synthesis process was carried out in a100 or 300 mL beaker and all the reagents were analytical grade to avoid further purification. In this method, Titanium Tetraisopropoxide (TTIP) with the chemical formula $Ti\{OCH(CH_3)_2\}_4$ was used for the titanium source and ferric nitrate ($Fe(NO_3)_3.9H_2O$) was used for the iron (Fe^{3+}) source as a precursor. In this synthesis process, anhydrous ethyl alcohol was used in the beaker at room temperature as a solvent. Ferric nitrate (0.5% Fe : Ti molar ratio) was dissolved in deionized water maintaining Ti : H_2O at 1:4. This solution was added either in 30 mL or 300 mL of solvent in a beaker depending on crystal production. The gel formation process was carried out in an acidic solution and HNO_3 (Nitric acid) was added dropwise to maintain a pH level of 3 to keep the mixture clear. During the whole gel formation process, a magnetic stirring bar was used to keep the solution in continuous mixing. In this acidic solution, TTIP was added dropwise at room temperature while vigorous stirring was continued for 2 hours till the gel formed [70]. Depending on the final state of the product, the next steps were slightly different from each other. To get powdered nanocrystals, this gel was dried at 80 °c for around 3 hours. The dried gel takes the form of as shown in figure 3.1.

Figure 3.1 Dried gel after 2 hours of drying at 80° C.

This dried gel was crushed into fine powder to ensure maximum removal of carbon residual accomplished by centrifuging 4 times and washing with deionized water. The washed powder was then calcinated at 400 °c with a temperature gradient of 10°c/min to get crystalized Fe-TiO_2. During this crystallizing process, single crystals of Fe-TiO_2 cluster together and form big agglomerates with contamination layers of iron oxides on the crystal surfaces. The clusters of Fe-TiO_2 were grounded in a mortar to get the minimum average size of the clusters as possible. For a further breakdown of these clusters, the powder was then sonicated at 80Hz in the alcoholic medium for 30 minutes. Sonicated crystalline powder was then stirred in concentrated HCl solution for 3 hours, centrifuged and washed 4 times to dissolve the iron oxide from the surface of the crystals. A flow chart of the synthesis process of doped TiO_2 is given below in figure 3.2 [70].

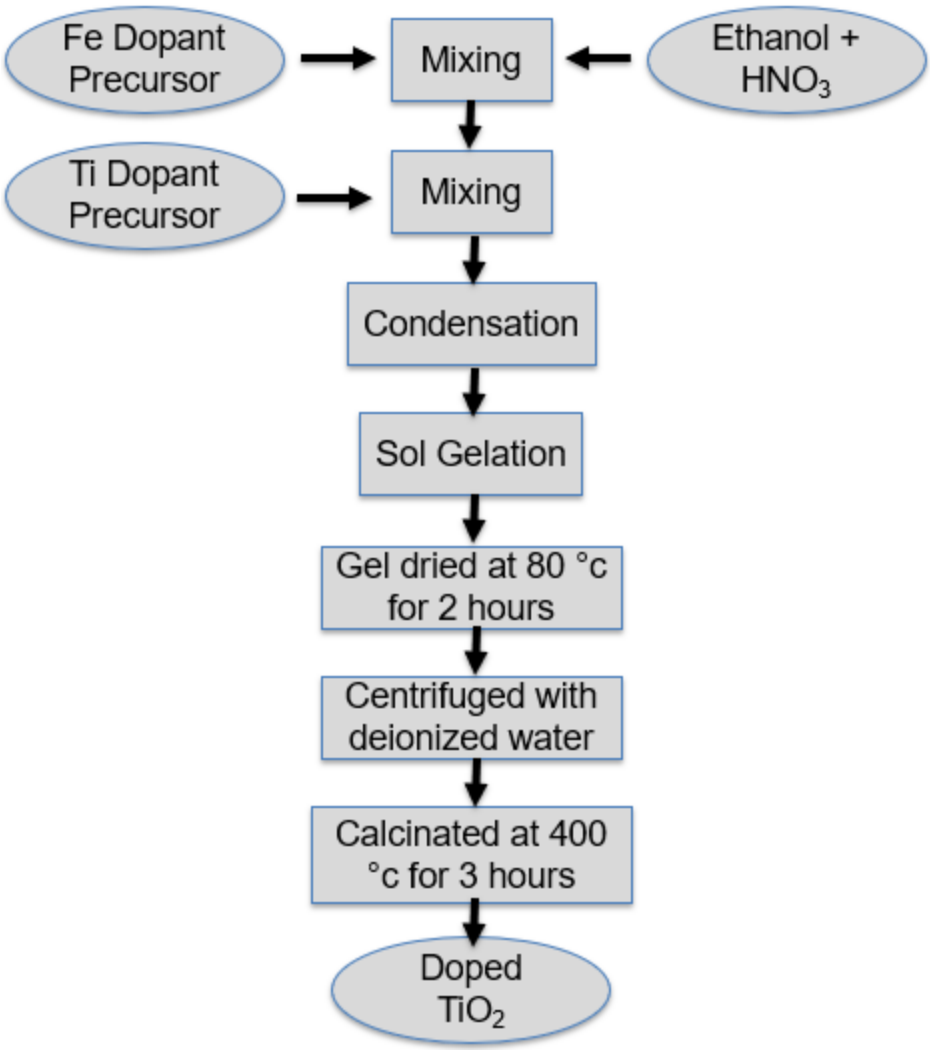

Figure 3.2 Flow chart of Fe Doped TiO_2 synthesis.

3.2 Attachment to fiberglass cloth

Different approaches were conducted to attach the Fe-TiO_2 crystals onto fiberglass cloth. Before coating, the very important step was preparing the condition of the cloth. A properly measured fiberglass cloth was cauterized all the edges with an oxy-acetylene torch to avoid the fiber thread from coming off the cloths. Some concerns were given importance while coating the fiberglass cloth. They are:

- Immobility of the crystals on the cloth surface
- Crystal/ crystal-cluster density on the cloth
- Operability of cleaning/washing prior to calcination

3.2.1. Dip coating:

The most conventional way of coating the fiberglass cloth is dip coating. In this process, the cleaned fiberglass cloth was dipped in the sol-gel until it properly wet both sides of the cloth. The cloth was then dried at 80 degrees for 2 hours. As it was quite impossible to centrifuge the cloth with the existing lab facilities to get rid of the carbon residue from the cloth, the dried sol-gel coated cloth was then immersed in deionized water and left it there for 4-5 hours. However, short-time washing caused a black surface on the glass slide after the calcination process because of carbon contaminants in the dried sol-gel as shown in Figure 3.3.

Figure 3.3 Carbon contaminated Fe-TiO_2 coating on glass slides

The washed cloth was then calcinated for 3 hours at 400° C. After 3 hours of calcination the Fe-TiO2 coated fiber-glass cloth was then acid-treated (concentrated HCl) for 3 hours to get rid of excess iron and iron oxide layers from the surface of the crystals/ crystal clusters. The entire dip-coating process from sol-gel can be schematically illustrated in figure 3.4.

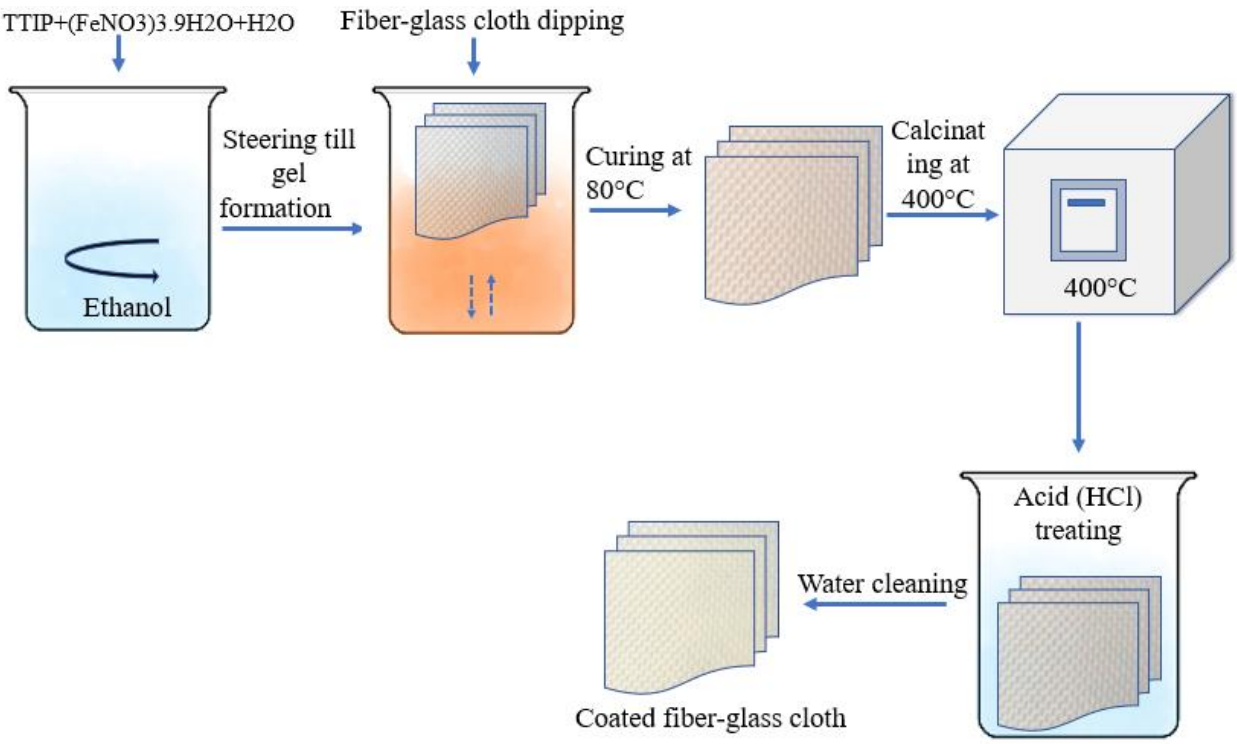

Figure 3.4 Schematic representation of the different stages of the dip-coating process from the sol-gel method.

The coated fiberglass cloth by this method showed a nonuniform thickness of TiO_2 layers on different parts of the cloth. When the calcined TiO_2 was cooled down to room temperature with the temperature gradient of 10° C/min, the coated TiO_2 cracked, which exposed more active surface area in the material.

3.2.2. Recrystallizing Fe-TiO2:

In this coating process, all the steps were followed exactly the same as described in the synthesis section. Besides, a suspension was made with the deionized water and the finely grounded crystal clusters. Then, the desired amount of fiberglass cloth was soaked in the thick suspension. When the entire fiberglass cloth was uniformly dispersed with the suspended crystals, the cloth was then recrystallized at 400°C for 3 hours. Finally, the crystal-coated cloth was washed and cleaned in

water followed by an acid (concentrated HCl) treatment. A schematic flow depicts the recrystallized coating process as shown in figure 3.5.

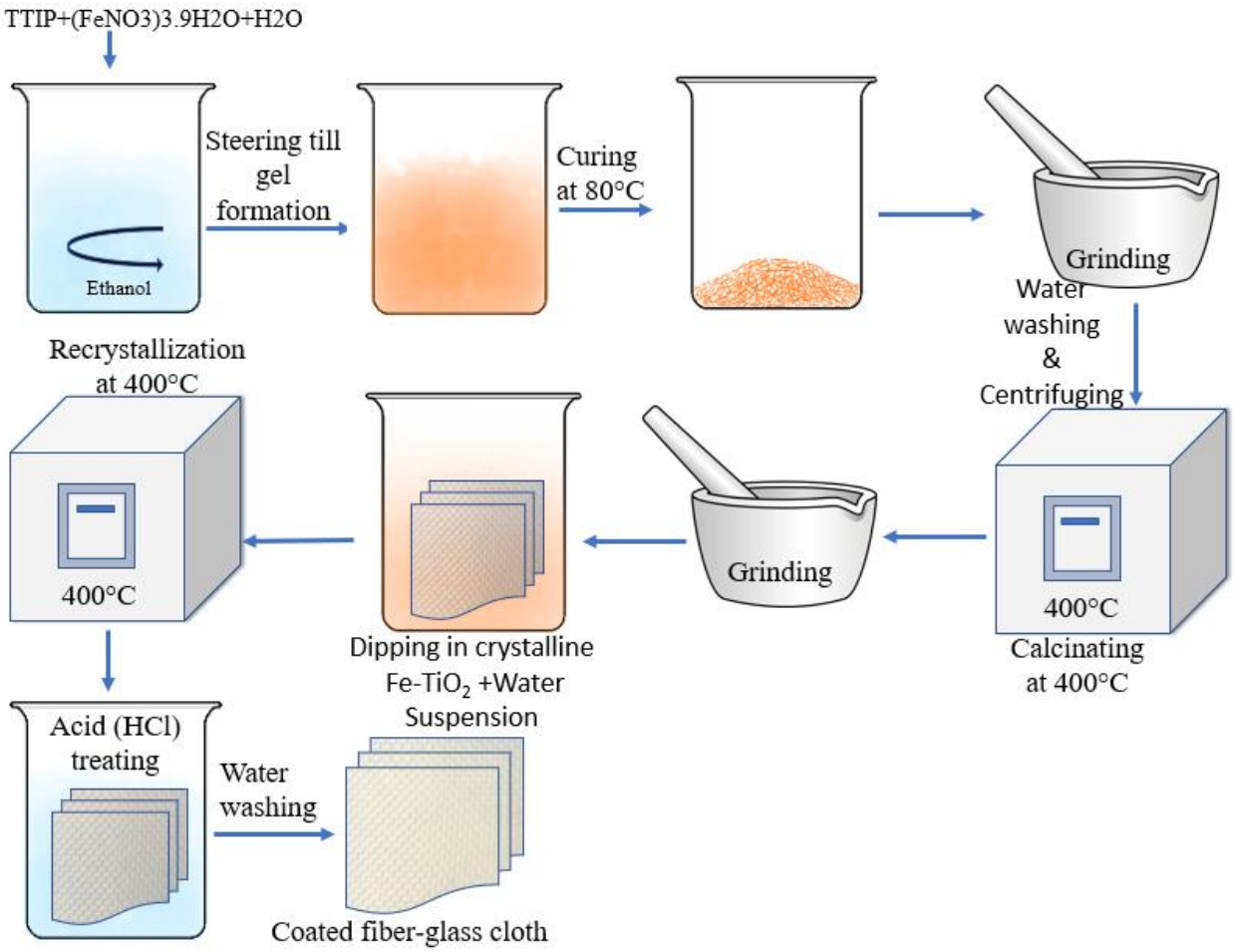

Figure 3.5 Schematic representation of the different stages of the recrystallized coating process from sol-gel.

In this process, smaller crystal particles could get in-between the fiberglass thread and the bigger clusters mostly stay on the surface of the threads.

3.2.3. Sintering dried gel powder:

In this technique, the crystal synthesis process was followed up to washing and centrifuging the dried gel powder as described in the synthesis section. After that, a thick suspension was made in

water with the washed and centrifuged dried gel powder. The pre-prepared cloth was then dipped and soaked in the thick suspension until most of the particles were absorbed by the cloth. Then the cloth was left in a high-temperature oven at 400° c for 3 hours. When the crystallization was completed after 3 hours, the cloth was treated with the concentrated HCl acid for 4-5 hours to eliminate the oxides and irons from the crystal surfaces. During recrystallization, smaller clusters were sucked in between the threads and the bigger particles attached on the top of the fiberglass cloth.

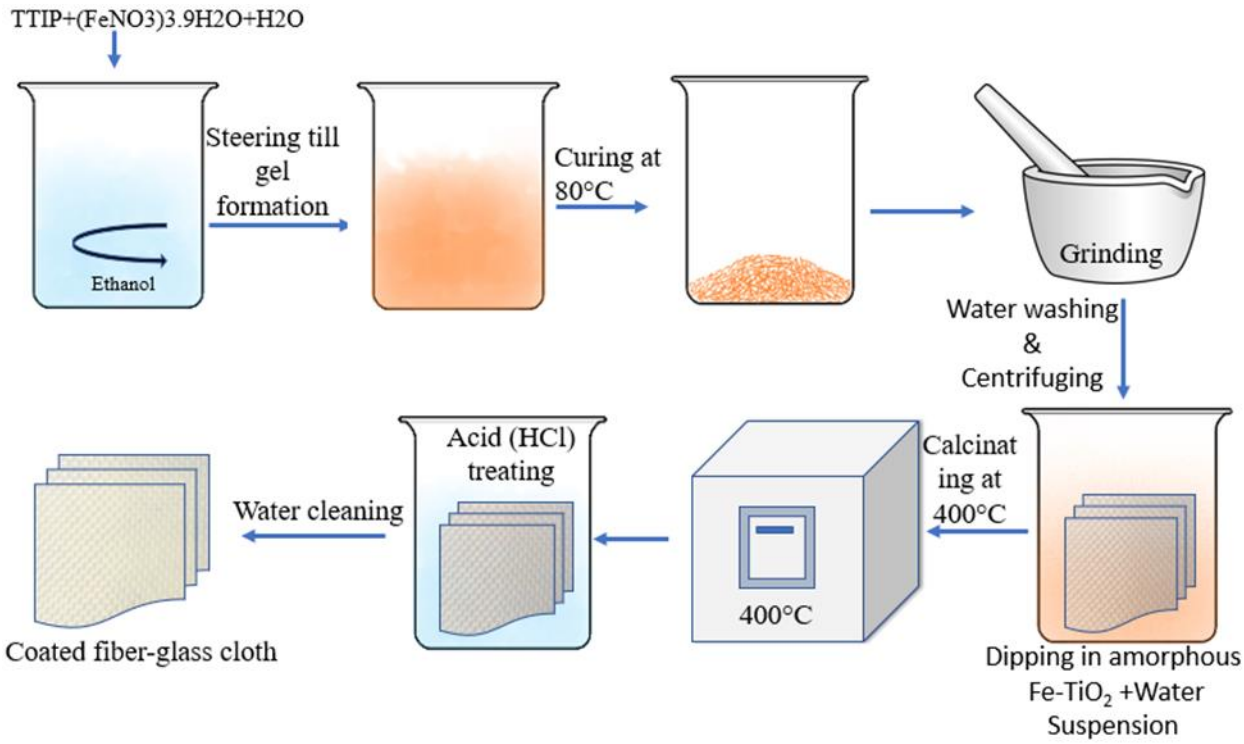

Figure 3.6 Schematic illustration of coating fiberglass cloth by sintering dried gel powder.

3.3 Application to wastewater cleaning reactor

To fulfill the aim of this project a prototype photoreactor was designed to take the photocatalytic wastewater cleaning technology from laboratory scale cleaning to commercial scale cleaning. There were several prototype photoreactors designed to serve the purpose of cleaning water. The design requirements of the photoreactor were to keep it simple so that it can be fixed, if necessary,

or even reproduced easily. Another intention to keep the design simple is to understand all the parameters related to water cleaning very easily. Here the photoreactor used for all the experiments is presented.

This photo reactor contains the following parts:

- 4 round bars (main support system)
- Two base rings (holds two disks from two ends)
- Two circular disks and (holds glass cylinder and the rectangular bars)
- A hollow rectangular bar (act as the light holder and heat sink)
- One glass cylinder and a wire mesh cylinder.

The CAD design of the photoreactor showed in figure 3.7 below.

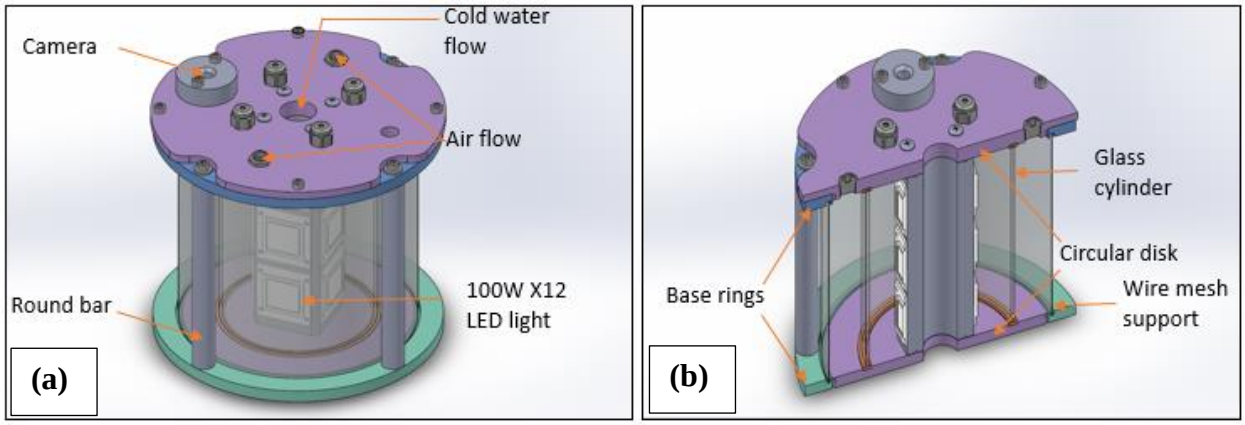

Figure 3.7 a) Computer-Aided Design (CAD) design b) Vertical cross-section of the photoreactor.

These 4 circular rods connect the base rings and act as the main support system of the photoreactor. The other two circular disk slides into the base ring at two ends of the reactors and forms a good seal. A rectangular hollow bar connects two disks and holds twelve 100W Light Emitting Diode (LED) lights, where 3 LEDs on each side of the rectangle to cover a 360-degree

illumination. Each of these blue LEDs emits light of wavelength between 395 nm and 405 nm and acts as a bright source of energy. When this 1200W light source was turned on, the heat produced by the light was conducted by the aluminum rectangular bar, a heat sink exchanging the heat to the water inside the bar. The hot water inside the cavity of the bar and the cold water outside of the cavity generate convective water flow from the bottom to the top of the reactor. For instance, the continuous flow of cold water keeps the lamps cool Another wire mesh cylinder was introduced in between four circular bars and the glass cylinder. The space between the glass cylinder and the wire mesh cylinder was filled with activated fiberglass cloth. One of the main components of this photoreactor is fiberglass cloth. Fiberglass was used because of its characteristic resistance against chemicals, dimensional stability, high tensile strength, high thermal endurance [71]. The pore size of the fiberglass cloth is around 200 µm (shown in figure 3.8).

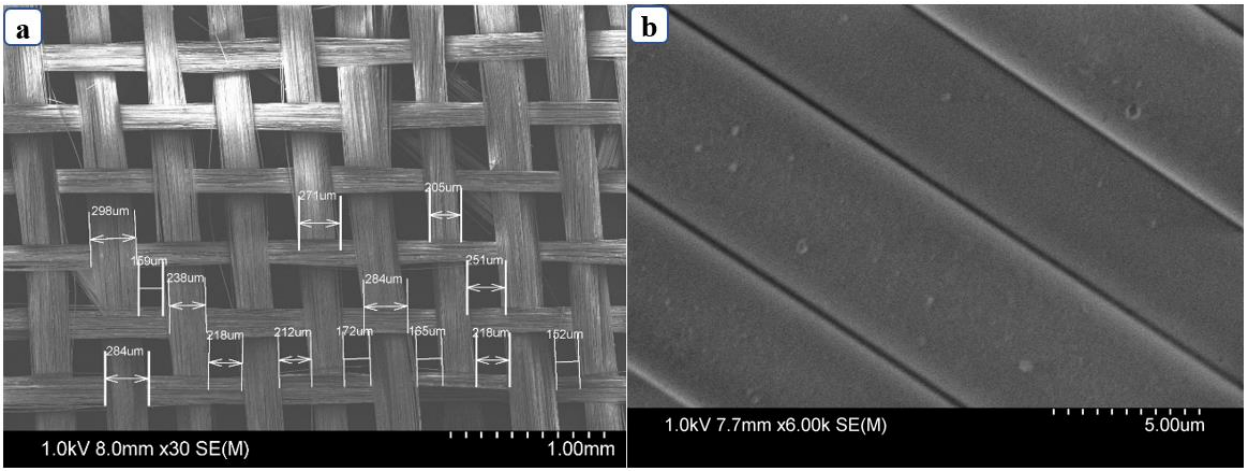

Figure 3.8 SEM image of a) fiberglass cloth with pore diameter and b) magnified fiberglass threads.

Three air inlets were introduced through the top disk of the reactor to create an air bubble in the reactor. These bubbles carry oxygen and mobilize ions and radicals towards the organic pollutants. A camera was installed on the top disk to monitor the functionality of the reactor.

Figure 3.9 Components of the photoreactors.

Flaws in the photoreactor:

- Three air tubes created strongly localized air bubbles that splashed water out of the water tank
- Few layers of fiber-glass cloth left an empty space between the two cylinders causes the cloths to flap when the air flowed.
- Few layers of fiberglass cloth contained insufficient crystals on their surface and generated a low ion current
- The heat produced by the lights eventually evaporated the water resulting in the pollutant concentration increasing in the water tank.

Modification in the reactor design:

There were some simple modifications done to avoid the problems faced during the experiments by the previous model. Eventually, the minor changes in design significantly enhanced the results.

- To control the evaporation of the solvent from the pollutant solution a heat exchanger was made by copper tube. An effective heat exchanger requires high thermal conductivity materials. Although copper suffers from a high value of the coefficient of thermal expansion (CTE), copper is most commonly used when materials of high conductivity are needed [72]. Continuous water flow was maintained through this tube to keep the entire wastewater solution at room temperature.

Table 3.1 A list of conventional heat exchanger materials and their CTE and density

Material	Thermal conductivity (W/m K)	CTE (10^{-6}/°C)	Density (g/cm^3)
Aluminum	247	23	2.7
Gold	315	14	19.32
copper	398	17	8.9

- Several layers (~10 layers) were rapped between the two cylinders to maximize the crystal density and to ensure maximum absorption of the light by the crystals as shown in figure 3.10. The reduced spacing between the cloths reduced the flapping of the fiberglass cloths in between the two cylinders. Hence, the condensed stacking of the coated fiberglass cloth more effectively immobilized the crystals on the fiberglass cloth.

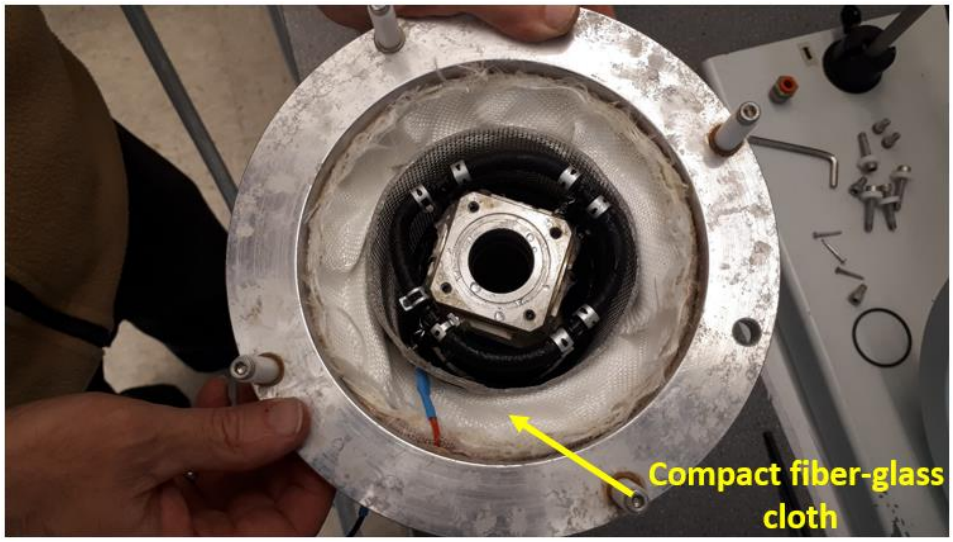

Figure 3.10 Open lid of the photoreactor with compact packaging of fiberglass cloth

- The bright intense light was partially transmitted through all of the coated fiberglass cloths. To trap the excess light that came out of the photoreactor, the outermost layer of fiberglass cloth was coated with gold nanoparticles. Depending on the thickness of the gold nanolayer the surface color of the fiberglass cloth varied from blue to yellow. Localized surface plasmon resonance (LSPR) of the gold nanoparticles resulted in a strong absorbance band in the visible light region. A long gold nanoparticle coated fiberglass cloth is shown in figure 3.11.

Figure 3.11 Fiberglass coating with gold nanoparticle by plasma coating technique.

- To avoid localized bubbling, splashing of water, and to provide uniform bubbles throughout the reactor tank a meshed system was made and placed around the lights. This mesh was made of Porous Irrigation Soaker Hose having an inner diameter of 0.6 cm. The presence of pores around the circumference of the tube made it an ideal source of bubbles that distribute the air uniformly all around the tube inside the photoreactor. The flow of cool air hit the flat LED lights likely reducing them getting warm.

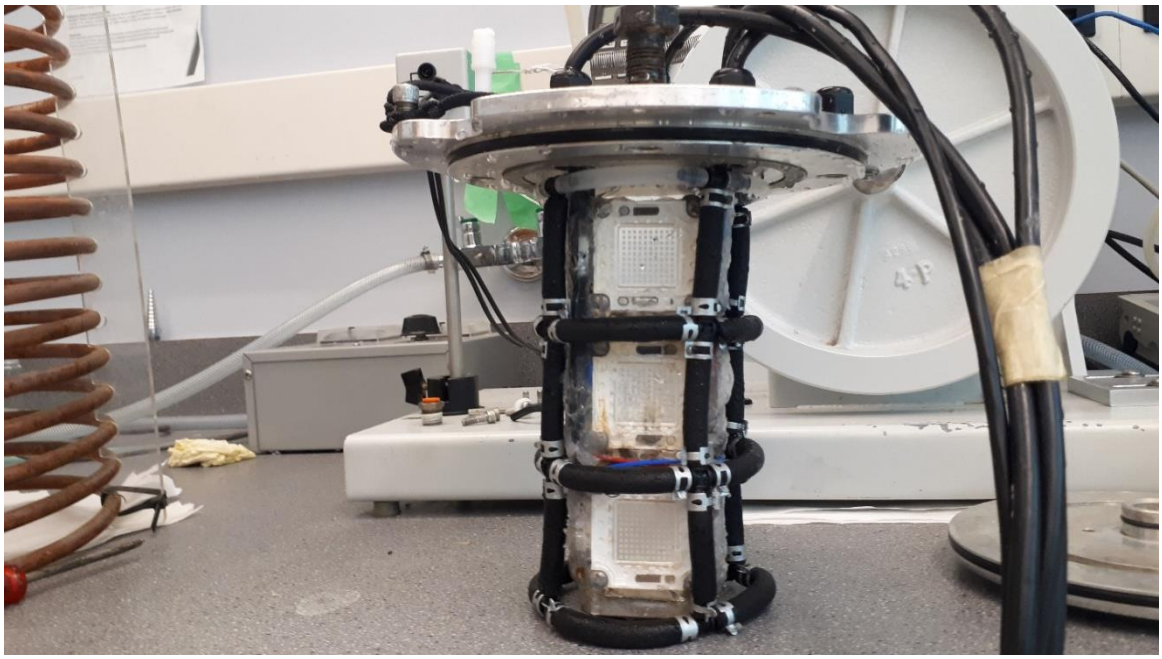

Figure 3.12 Porous tube aeration system of the reactor.

- Another important change in the reactor design was replacing the glass tube with another wire mesh cylinder of the same size. The main purpose was to incorporate electrolysis along with photocatalysis by making one of the wire mesh cylinders an anode and the other one as the cathode. An external source of voltage was connected in between the two electrodes and an ammeter was connected in series to observe the ion current flowing in the wastewater solution during its cleaning. This ion current indicates the number of oxidants produced by the reactor for cleaning purposes.

Chapter 4- Experimental Results

This chapter presents the experimental results collected during the development of the photoreactor. These results played a vital role in understanding the degradation of the wastewater process necessary to make changes for enhancing the rate of degradation. Firstly, a brief investigation was done by temperature-dependent crystal growth of Fe-TiO2 by XRD (x-ray diffraction) study, and a morphological study was done by synthesizing crystals under different cooling rates and environments. Secondly, several methods were tested to attach the Fe-Tio2 crystals onto fiberglass cloth, and finally, the coated fiberglass cloth was installed and tested in several reactor designs to clean model wastewater applying changes in the design dependent on the degradation of the pollutant as a function of time.

4.1 Fe doped TiO_2 crystals (show your XRD data)

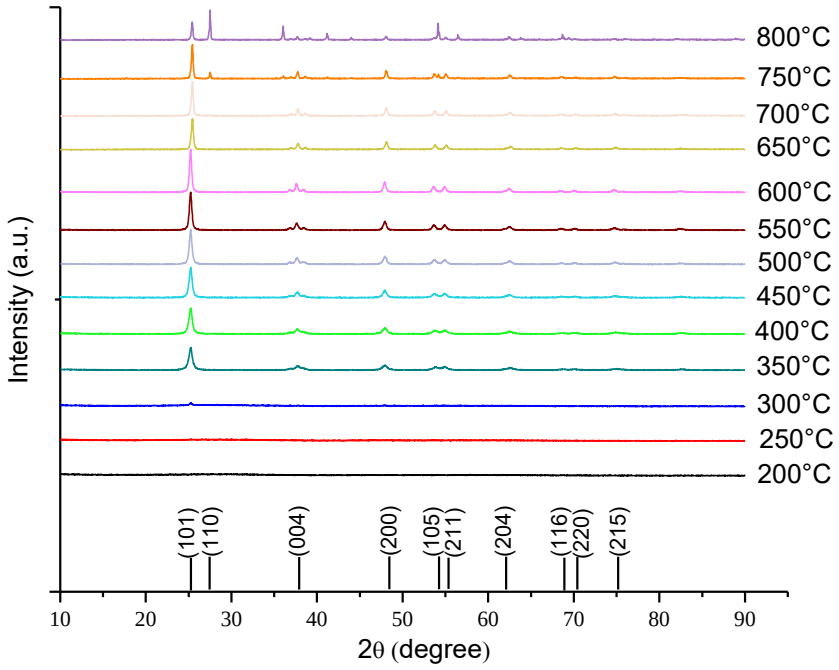

Figure 4.1 Non-ambient X-ray diffraction (XRD) patterns of $Fe_{0.5}$- TiO_2 phase transformation with the function of temperature, ranging from 200 to 800°C.

XRD diffraction patterns of Fe-TiO_2 were performed using a Panalytical Empyrean X-ray diffractometer (XRD) with copper X-ray lamp, Kα (*A*°) = 1.54. In these measurements, phase transformation was studied for 0.5 molar % Fe in Fe-TiO_2 within the temperature range of 200-800°C. From figure 4.1, it is observed that at 300°C the main peak of anatase representing the (101) crystal plane started to appear at a 2θ value of 25.3° [73]. There was no change in the crystal phase with the increase of temperature up to 700° C but when it reached 750°C the (110) peak intensity of rutile appeared at 2θ value of 27.50° [74].

From the plot at 400°C, the Bragg diffraction peaks were observed at 38.0, 48.1, 54.0, 55.1, 62.1, 68.8, 70.2 and 75.1° corresponding to (004), (200), (105), (211), (204), (116), (220) and (215) crystal planes of anatase, respectively [75], [76]. The maximum Bragg diffraction was observed from the planes at 400°C afterward used for the calcination temperature of Fe-TiO2.

4.2. Influence of Fe-TiO_2 crystal cluster size in photoactivity

Physical properties (e.g., crystal structure, surface area, surface hydroxyls, and particle size) of synthesized TiO_2 greatly influence the photocatalytic activity of degrading organic pollutants in suspended solution [77][78][79]. The morphological observation was done on synthesized crystals to study the influence of crystal cluster size on degradation efficiency of wastewater. With a decrease of TiO_2 crystal size, degradation efficiency increases [80] due to the smaller particle having a higher surface area. Due to the higher crystal surface area, more photo-ion-current can be produced during the illumination of light to produce more ˙OH radicals. The more ˙OH radicles in the wastewater solution, the faster will be the degradation.

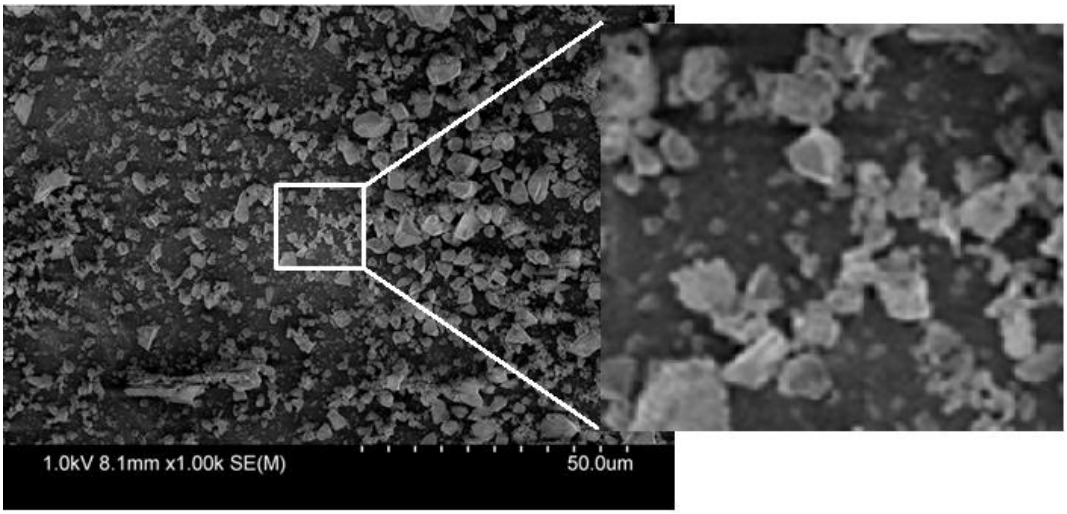

Figure 4.2 SEM image of synthesized $Fe_{0.5}$-TiO_2 crystals/crystal clusters.

Even though the single-crystal size was measured to be about 10 nm [8] the calcined crystals exist as aggregate clusters consisting of single crystals having a range in size (Figure 4.2). A Hitachi S-4800 FESEM (Field Emission SEM) was used to study the morphology of the synthesized crystals. To investigate the Fe0.5-TiO_2 crystals/crystal clusters morphology a diluted suspension was made with a Fe0.5-TiO_2 powdered sample and 100% ethanol. Following ethanol evaporation, prepared SEM stubs having crystals were sputter-coated with carbon using Cressington 208 sputter coater in order to reduce charging effects.

SEM images revealed that the traditional dry grinding process for the calcined powder produces crystal clusters mostly in the range of 250-500 nm and a significant amount of cluster size was between 1-2.5 μm.

Table 4.1 crystal/ crystal cluster size range in a conventionally prepared sample.

Crystal/Aggregate	**Size**
$Fe_{0.5}$-TiO_2 single crystal	~10nm (XRD)
$Fe_{0.5}$-TiO_2 Aggregate	~30nm to ~10μ (SEM)

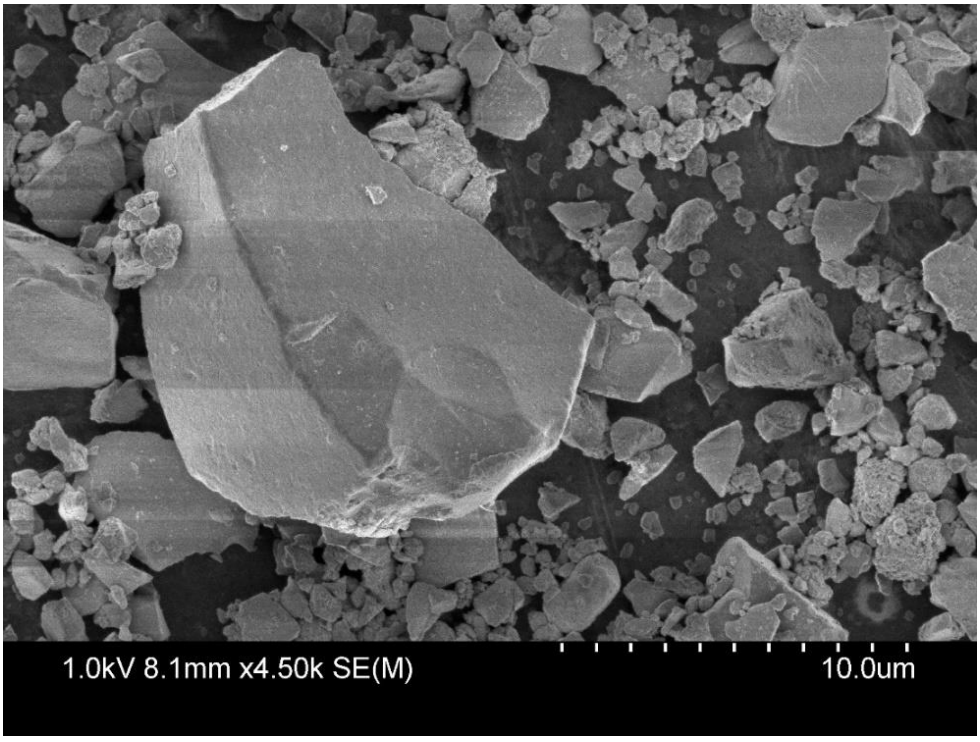

Figure 4.3 SEM image of traditionally prepared dry grounded Fe0.5-TiO2 sample.

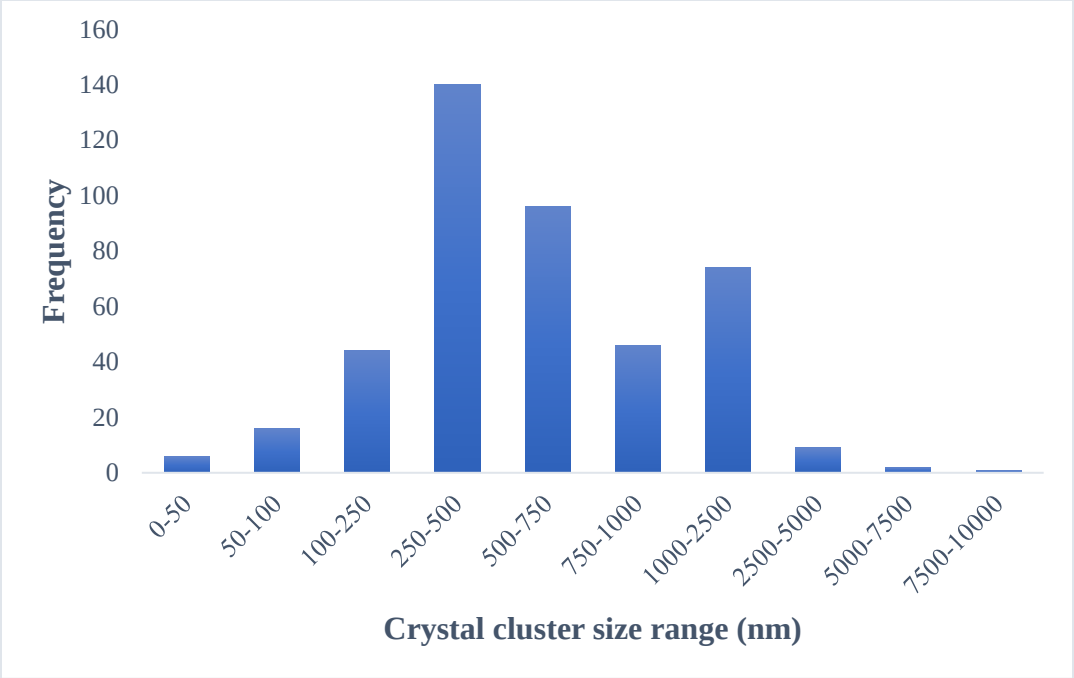

Figure 4.4 Traditionally prepared dry grounded Fe0.5-TiO_2 crystal cluster's size distribution.

Another sample preparation technique was employed to break down the crystal aggregate by using sonication followed by wet grinding. The solvent viscosity and surface tension have great influence in sonication as they control the cavitation phenomenon, i.e., the higher the cohesive forces within a liquid, the more difficult is the cavitation [81][82]. When cavitation happens close to an extended solid surface, cavity breaks down and generates high-speed jets of liquid on to the solid surface [83][84]. During the ultrasonic irradiation of the liquid-solid suspension, the resultant jets and associated shockwave along with high-velocity inter-particle collisions are capable of inducing a massive change in surface morphology [85]. The solvent with Lowe Surface Tension generates a cavitation bubble more easily than a liquid with higher surface tension. At room temperature surface tension of ethanol (22.2 dynes/cm) is significantly lower than the water (72.6 dynes/cm) [86].

After wet grinding in a thick suspension of calcined powder in ethanol solvent and sonicating in ethanol solvent for 30 minutes, SEM images reveal a noticeable change in crystal cluster morphology. A total of 670 crystal clusters were observed to measure their size manually from SEM image by using an open-source image processing software named ImageJ. The plotted statistical data has a standard deviation of 87, which is higher than the previous set of data meaning that the particle size is widely distributed and the maximum number (255) of the clusters were in the size range of 100-250 nm.

Table 4.2 crystal/ crystal cluster size ranges after wet grinding and sonication in alcoholic media.

Crystal/Aggregate	**Size**
Fe0.5-TiO_2 single crystal	~10nm (XRD)
Fe0.5-TiO_2 Aggregate	30nm to ~1μ (SEM)

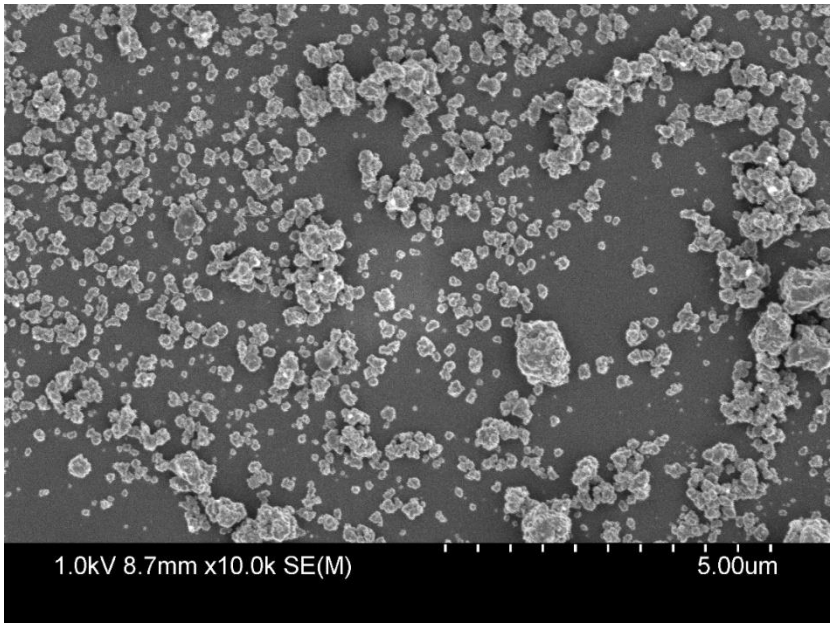

Figure 4.6 SEM image of wet grounded, sonicate, and acid-treated TiO_2 crystal clusters.

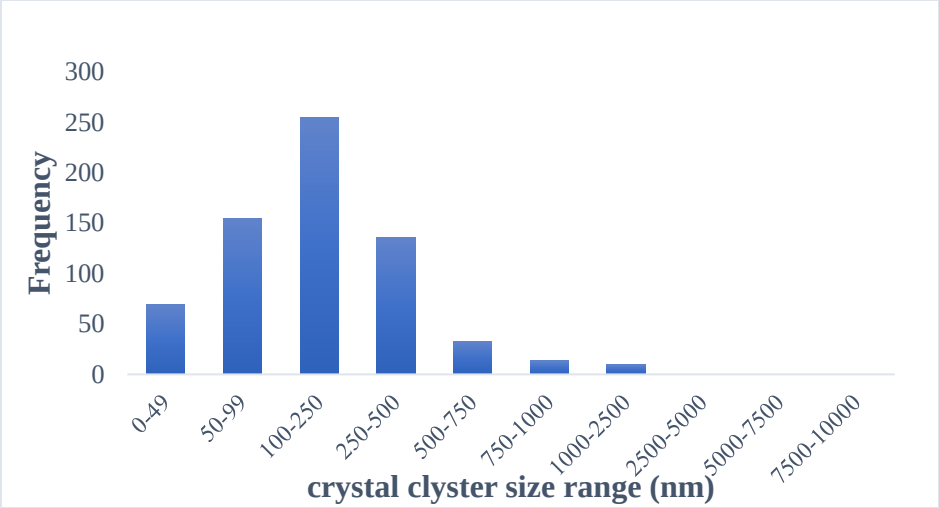

Figure 4.7 Wet grounded and sonicated $Fe_{0.5}$-TiO_2 crystal cluster's size distribution.

To test the effectiveness of this alcohol wet grinding and sonication technique on photocatalytic degradation of pollutant more experiments were conducted where a number of wet grinding, sonication, and acid washes were the variance. Photocatalytic activity of three sets of Fe-TiO_2 samples was measured and 10 ppm phenol was used as the model pollutant. The number of repetitions of grinding and acid cleaning in sample preparation to break down existing bigger clusters to the finer particle eventually increases the net surface area of the crystals. With the increased surface area, the photocatalytic activity also increased, and hence the degradation of pollutants happened faster; meaning the concentration of the pollutant decreased more rapidly. As the concentration decreased the color of phenol gets milder and results in low absorption of UV-vis light from the spectra (figure 4.8). In short, the larger the surface area the more active are the crystals and the lower will be the absorbance over time. The plot depicts that over 90-minute duration of reaction time triple grounded, sonicated and acid-washed crystal clusters achieved the highest degradation efficiency of around 85% having a maximum standard error of ±1.11 with 95% confidence level, shown in figure 4.9. Figure 4.10. demonstrates the rate constants of single, double, and triple grounded and acid-treated $Fe_{0.5}$-Ti_{O2}.

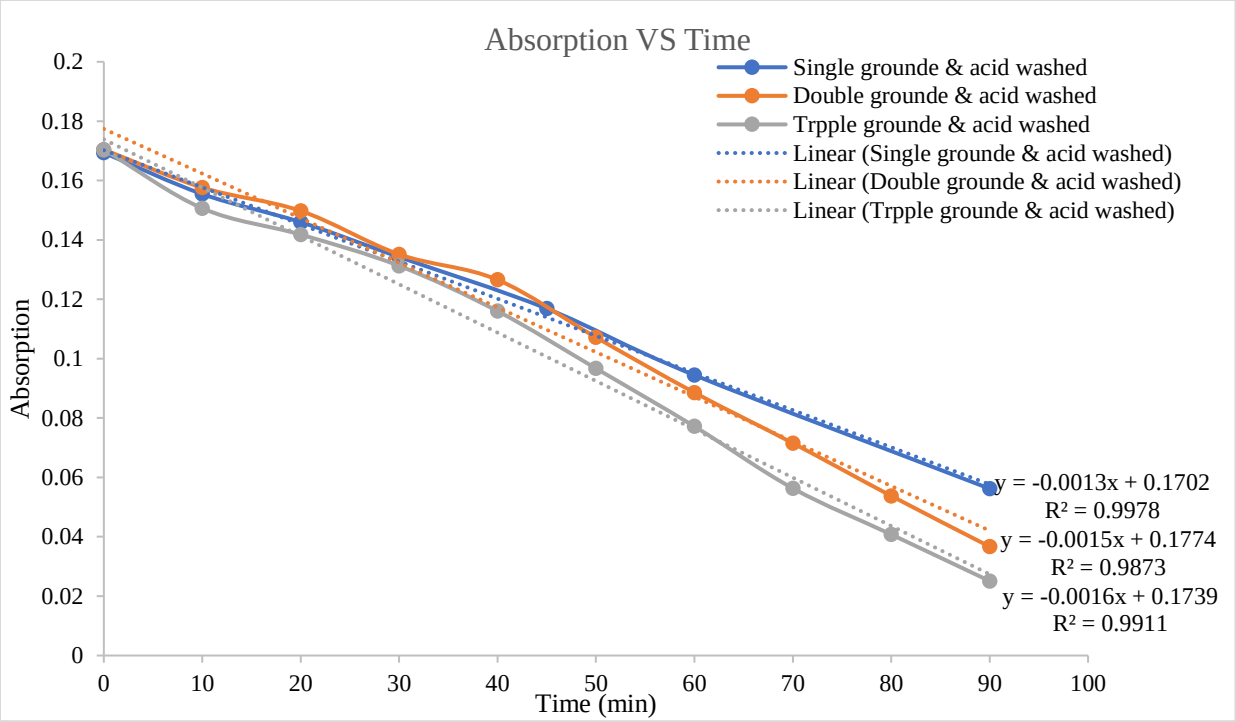

Figure 4.8 Visible light absorbance of phenol, degraded with single, double, and triple time grounded and HCl cleaned $Fe_{0.5}$-TiO_2.

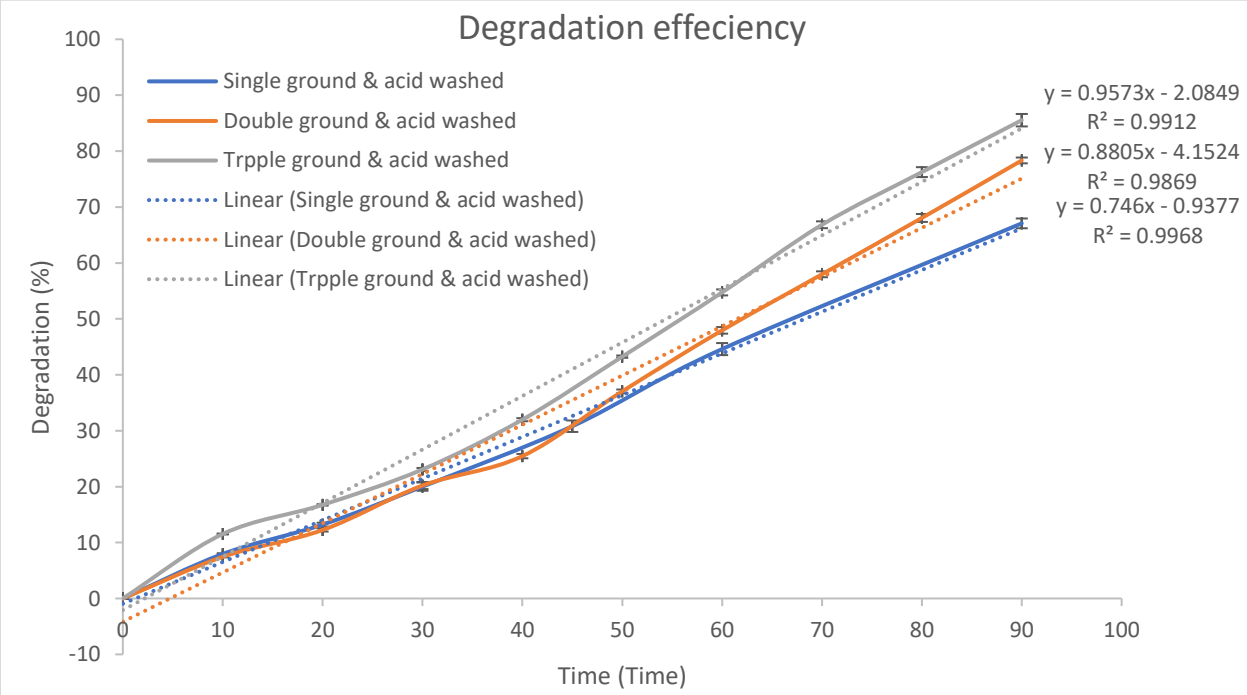

Figure 4.9 Influence of grinding time and acid cleaning on degradation efficiency of $Fe_{0.5}$- TiO_2 using 10 ppm of phenol solution within 90 min of reaction time under visible light illumination.

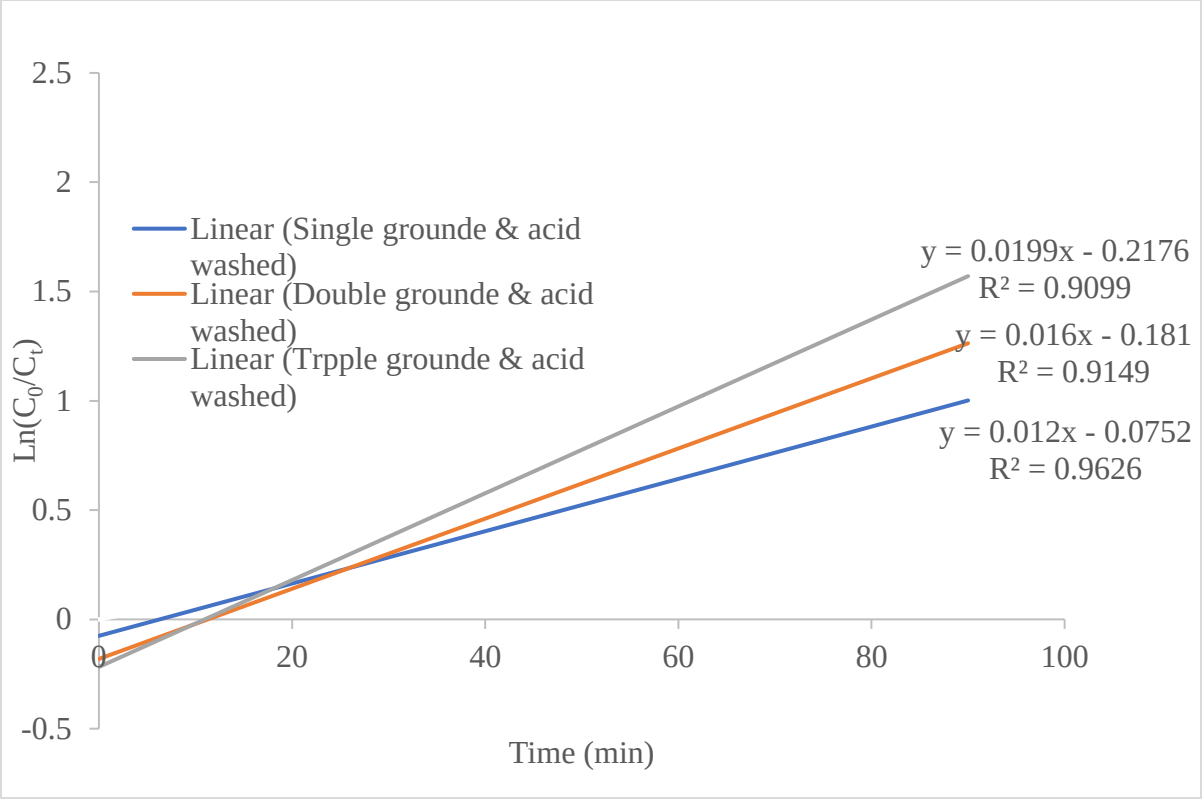

Figure 4.10 Rate constant of single, double, and triple grounded and acid-treated $Fe_{0.5}$-Ti_{O2} under visible light illumination within 90 minutes.

Table 4.3 shortly documented the number of grinding and acid cleaning results on phenol degradation.

Table 4.3 Effect of multiple cleaning and grinding on Phenol Degradation.

Experiment #b	Grinding time	Acid (HCl) Cleaning time (min)	Degradation (%) in 90 min	Standard error at 90 min	Confidence level (95%) at 90 min	
					Lower confidence interval (95%)	Upper confidence interval (95%)
1	10	180	67	0.87	63.32	70.84
2	20	360	78	0.52	76.09	80.58
3	30	540	85	1.11	80.74	90.33

4.3 Attachment of crystals to fiberglass cloth

In the next stage of the research, to scale up the wastewater cleaning from a small scale (100 ml) to a relatively large volume of wastewater (16000 ml), a photoreactor was designed. In this photoreactor, porous soda-lime fiberglass cloths were used to immobilized TiO_2 crystals

essentially preventing their loss to the environment. Fiberglass cloth is commonly used for its characteristics of high surface area, lightweight, low cost, transparency for natural light, relative chemical inertness, and exceptional pH and thermal stabilities. Moreover, the physical properties of fiberglass cloth enable it to be flexible, which allows it to be tailored into different sizes and folded into many shapes. Therefore, fiberglass cloth can be used appropriately in different photoreactor configurations for practical applications [87], [88], [89], [90].

The SEM image of conventional dip coating on fiberglass cloth revealed a very good surface coverage over the fiberglass cloth. The dip-coated fiberglass cloth offered a rigid bonding of the $Fe_{0.5}$-TiO_2 crystal clusters onto the fiberglass cloth. The $Fe_{0.5}$-TiO_2 crystal clusters also grow into the cloth pores like teeth. During the calcination, the solvent evaporated fast leaving a cracked surface appearance on the cloth.

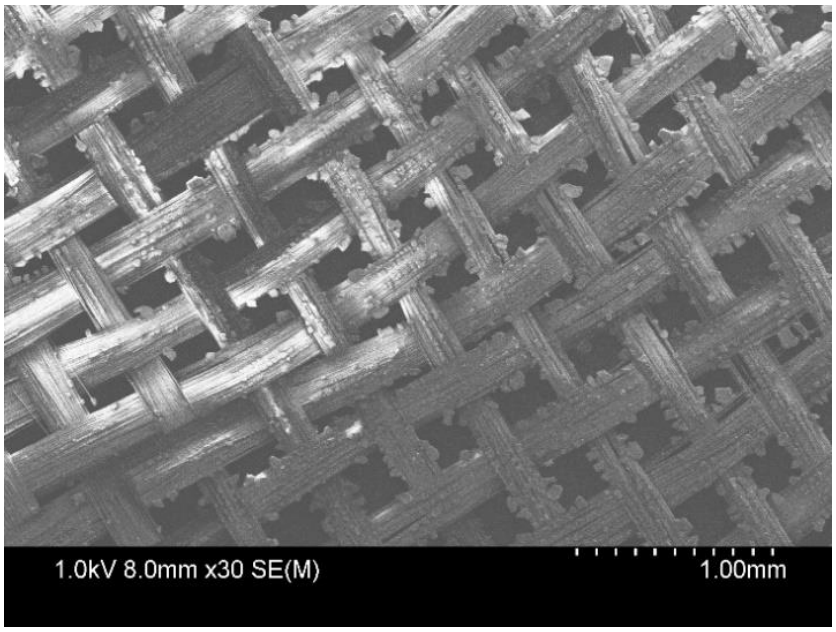

Figure 4.11 An SEM image of dip-coated fiberglass cloth.

It was assumed that because of the hanging cluster in the pores and the cracks on the fiber-glass cloth there would be an increase in the net surface area and hence there would be a decent degradation of sample pollutants upon light illumination. In the first set up of the photo-reactor, 0.444 m^2 of cloth was coated with approximately 7 g/m^2 of $Fe_{0.5}$-TiO_2 crystal density. In this experiment, there were twelve 100 w white LED lights used and no heat exchanger to keep the unit cool. No degradation was found but rather an increase in the concentration of the pollutant was observed over the 24 hours of reaction time. From graph 4.12, it can be seen that in the first hour only around 2% of pollutant degraded and then the pollutant concentration started to increase with time due to evaporation.

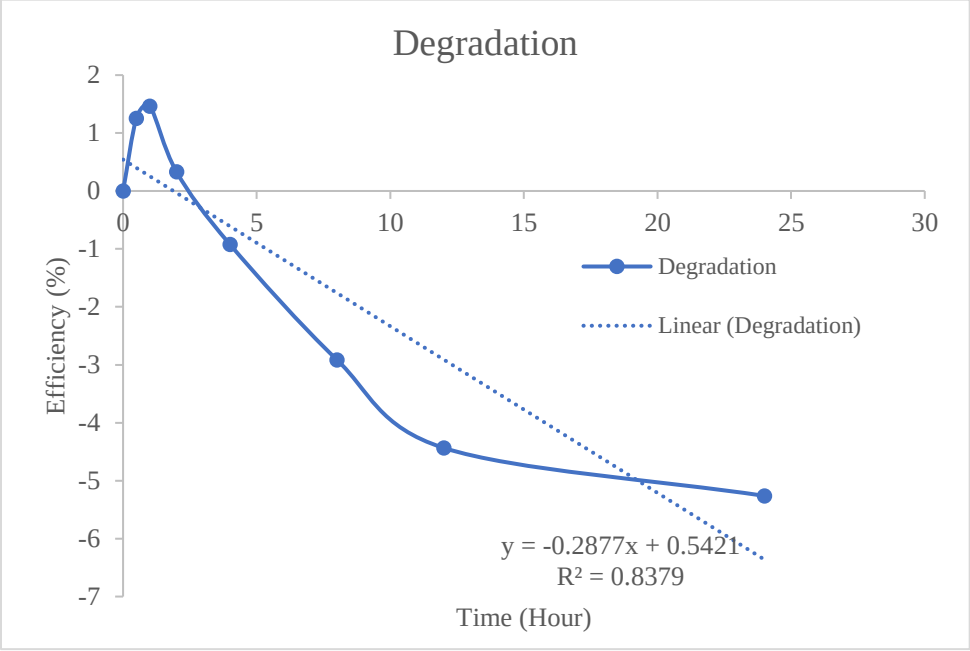

Figure 4.12 Degradation efficiency of the photoreactor that used dip-coated fiberglass cloth of $Fe_{0.5}$-TiO_2. [MO]= 5 ppm and crystal density 7 gm^{-2}.

- It was not possible to clean off all the remaining carbon residue from the dip-coated fiber-glass cloth that led to contamination in anatase crystal of Fe-TiO_2. This contamination disabled the functionality of the crystals.
- 12000W LED light (12X100W) generated enough heat to evaporate the pollutant solvent from the reactor bath and over 24 hours about 10 litters of solvent water were lost.
- The high-speed airflow into the reactor caused bubbles that splashed fluid out of the bath causing a heavy loss of water.

Another experiment was done replacing the white LED with a relatively broader light spectrum (<495) and adding a heat exchanger (spiral copper tube with cold water flow) around the reactor in the bath. After attempting an unsuccessful experiment, it was decided to start with a lower concentration of pollutants ($5mgL^{-1}$) in 16L of water and increased surface area of cloth ($0.986m^2$) with about $5g/m^2$ of crystal density on it. This time the fiberglass cloth was coated by the second coating technique, i.e., recrystallization of Fe0.5-TiO_2 onto fiberglass cloth, which has a cleaner, contamination-free activate surface (Figure 4.13).

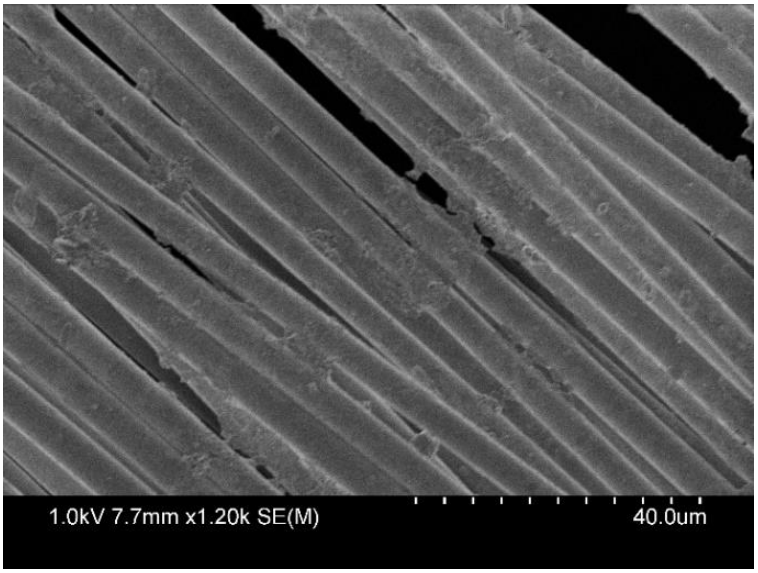

Figure 4.13 SEM image of coated fiberglass cloth by recrystallized technique.

The second experimental result depicted an overall 56% degradation efficiency of the photoreactor. The rate of degrading pollutants was higher in the first 10 hours and then the degradation rate falls off.

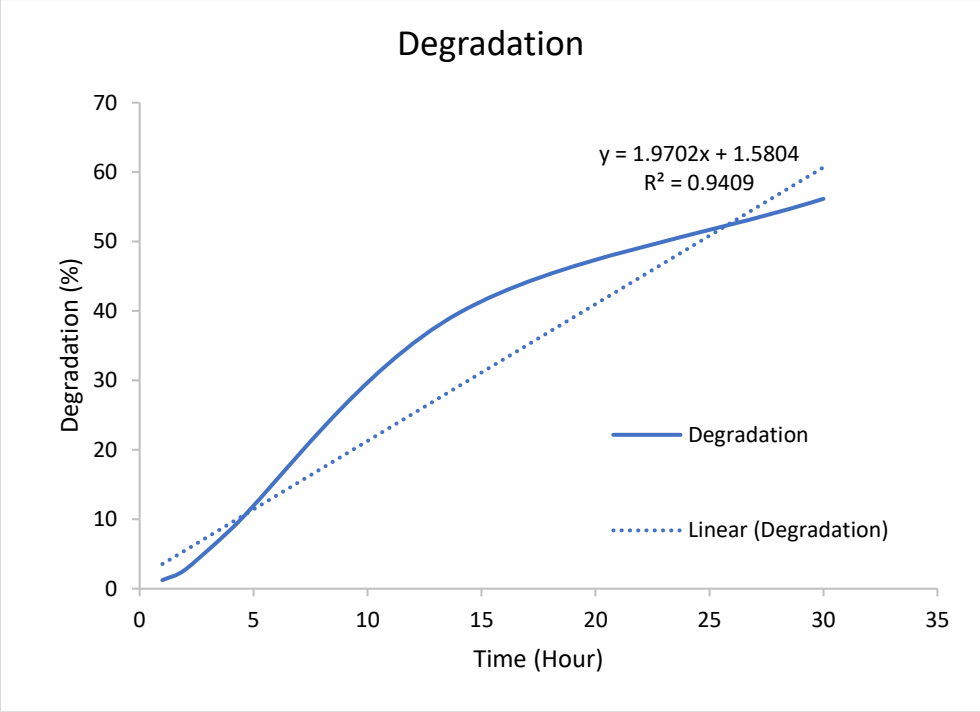

Figure 4.14 Degradation efficiency of the photoreactor that used recrystallizing method to coat fiberglass cloth with $Fe_{0.5}$- TiO_2. [MO] = 5 ppm and crystal density 4.7 gm^{-2}.

Another degradation experiment was conducted using the sintered dry gel method of coating. This time 1.609 m^2 of fiber-glass cloth was used with a crystal density of about 13 g/m^2 and the initial pollutant concentration was increased from 5 ppm to 20ppm.

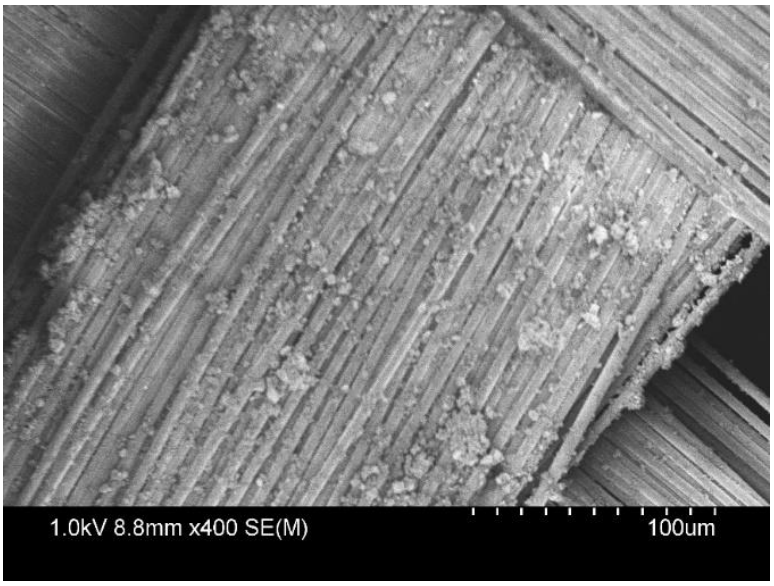

Figure 4.15 SEM Image of fiberglass cloth coated by sintering dried gel TiO_2 powder.

Over 34 hours of reaction time the photoreactor achieved 34% of degradation from its primary pollutant concentration. The regression coefficient is 0.9982 that is close to 1, meaning almost constant reaction rate during this 34 hour.

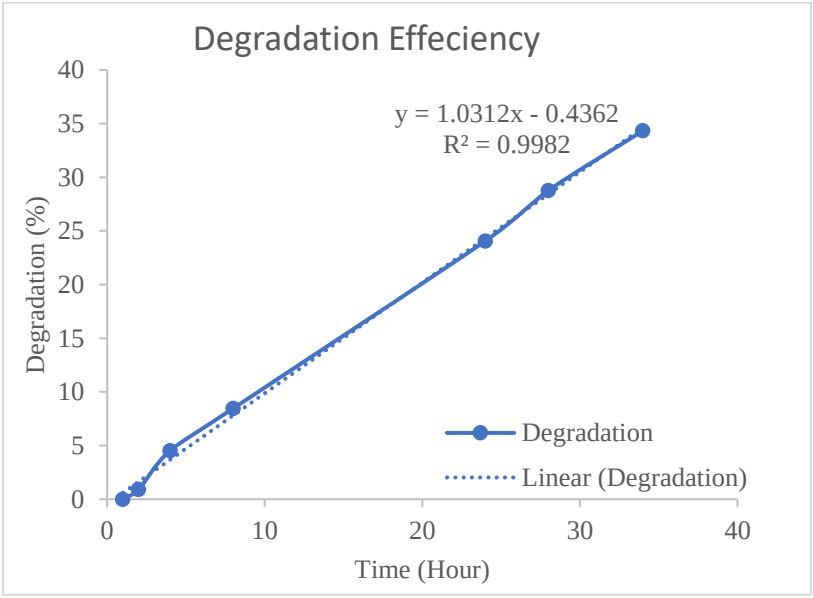

Figure 4.16 Degradation efficiency of the photoreactor that used recrystallizing method to coat fiberglass cloth with $Fe_{0.5}$- TiO_2. [MO] = 20 ppm and crystal density 13 gm^{-2}.

Table 4.4 A summary of three coating techniques.

Sol-gel coating method	Crystal density (g/m^2)	The surface area of the cloth (m^2)	The concentration of the pollutant (ppm)	Volume loss (L)	Degradation efficiency after 24 hours
Dip coating	7	.444	5	8	0.00
Recrystallizing	4.7	.986	5	10	56.15216
Powder sintering	13	1.609	20	5	34.332

4.4. Line analysis of coated fiberglass cloth

The interface and concentrations of Ti, Fe, Si, and Ox at the Fe doped TiO_2 – SiO_2 fiberglass cloth was imaged using field emission scanning electron microscopy (SEM) and by using its energy-dispersive X-ray spectroscopy (EDS) operating at 13 kV energy. A line analysis was performed on a suitable spot on the coated fiberglass cloth where a distinct crystal aggregate of $Fe_{0.5}$-TiO_2 was attached to a fiber of the fiberglass cloth (figure 4.18).

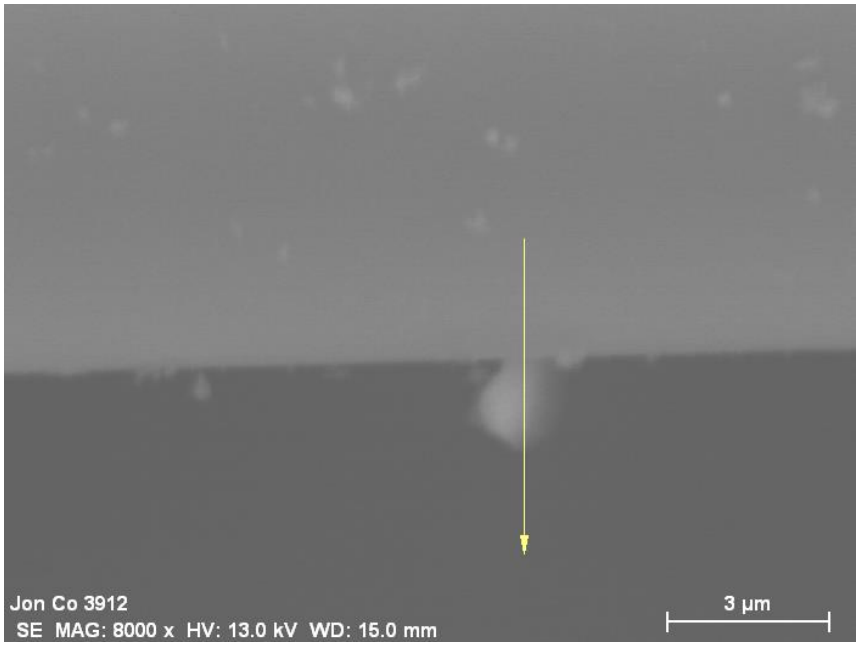

Figure 4.17 EDS line analysis and scan direction at the interface of fiberglass and $Fe_{0.5}$-TiO_2 specimen.

The EDS line scan showed the distribution of O, Ti, Si, and Fe along the direction from fiber-glass to $Fe_{0.5}$-TiO_2 cluster. The results show that the distribution of Si concentration is decreasing along the length of the arrow and at the interface of the glass and $Fe_{0.5}$-TiO_2, the Si concentration was minimum. The Ti concentration started to increase gradually from the interface into the crystal aggregate having the maximum peak height in the middle of the $Fe_{0.5}$-TiO_2 cluster. The corresponding EDS elemental line map (Figure 4.19) confirmed that Fe and Ti are only present in the $Fe_{0.5}$-TiO_2 crystal agglomerate. There was negligible diffusion of Ti, Fe, and Si between the soda-lime glass fiber and $Fe_{0.5}$-TiO_2 crystal.

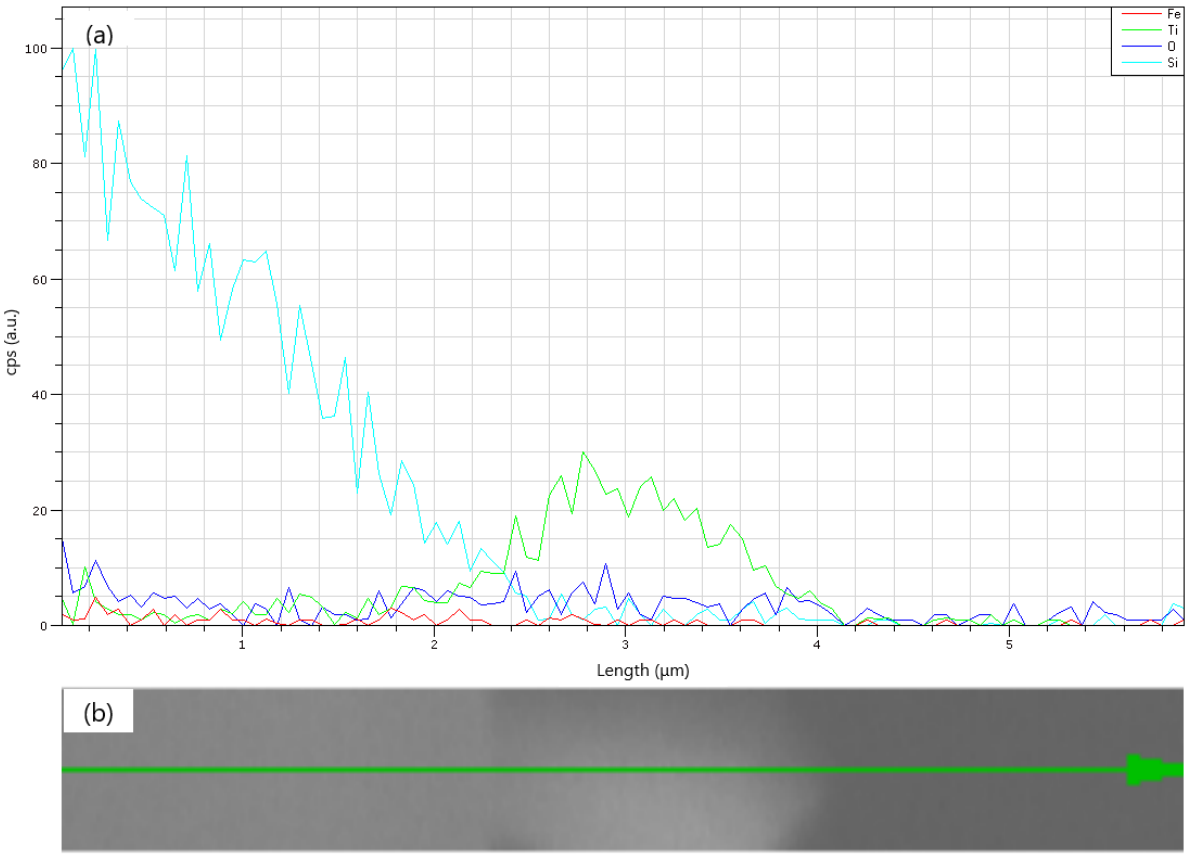

Figure 4.18 SEM–EDX line scans of $Fe_{0.5}$-TiO_2 coated fiberglass. (a) EDX plot shows the relative elemental content along with the line scan and (b) SEM image displays the position of the line scan.

4.5. Photo-ion current measurement:

The purpose of a photo-ion's current measurement was to understand the influence of different variances in a photoreactor through ion current production. To perform the experiments, a unique device named photo-ion current measurer was designed. This is a rectangular shaped cell with a partition in the middle. Each half of the cell has the capacity to contain one litter of water. Either side of the cell can be used as an independent electrochemical cell where two 4 cm^2 electrodes were placed vertically on top of each half of the cell with the minimum gap. A 100W blue LED light was placed just over the electrodes and the electrodes were connected with the DC terminal of a digital pico-ammeter. Each of the half-cells is equipped with an aquarium pump to circulate the water and a thermometer to track the temperature. Even a small change in the cell environment reflects the change in ion current in the cell. In one stage of the experiment, activated and non-activated fiberglass cloths were placed in between the electrodes in such a way that both electrodes touch the cloth. Change in any combination of the following variance in the table changes the ion current as shown in the table.

Table 4.5 A measurement of photo ion current by the photo ion current measurer.

Experiment Number	Pump	**UV Filter**	**light**	**Fiber-glass cloth**	**Current (μA)**
1	**OFF**	**X**	OFF	WITHOUT	0.705
2	**ON**	**X**	OFF	WITHOUT	0.43
3	**ON**	**X**	OFF	WITHOUT	-3
4	**ON**	✔	OFF	WITHOUT	.5 ± 0.02
5	**ON**	✔	ON	WITHOUT	-4 ±2
6	**OFF**	✔	ON	WITHOUT	-1.5 ± .5
7	**ON**	✔	ON	WITHOUT	2 ±2
8	**ON**	**X**	OFF	NON-ACTIVATED	.5 ± 0.03
9	**ON**	**X**	ON	NON-ACTIVATED	1 ± .03
10	**ON**	✔	OFF	NON-ACTIVATED	.5

11	**ON**	✔	ON	NON-ACTIVATED	1.7
12	**ON**	X	OFF	ACTIVATED	.75
13	**ON**	X	ON	ACTIVATED	1.5
14	**ON**	✔	OFF	ACTIVATED	.67
15	**ON**	✔	ON	ACTIVATED	-2

From the ion current in, the number of charges produced from the activated cloth can be calculated from the following equation:

$$I = \frac{Q}{t}$$

Where I represent ion current, Q as charge, and t as time.

Again, 1 Ampere = 1 Coulomb /1 Second

Charge on 1 electron = 1.6×10^{-19} Coulomb

By the unitary method, using experiment 7 and 15, the number of electric charges can be calculated as follows:

If 1.6×10^{-19} Coulomb / Second (Ampere) = Current by 1 electron

then, 4 µAmpere = 4×10^{-6}/ (1.6×10^{-19}) electrons

$=2.5 \times 10^{12}$ electrons.

i.e. 2.5×10^{12} electrons could possibly be generated when the visible light shines on a 4 cm^2 activated fiberglass cloth.

4.6. Wastewater cleaning reactor

Initially, the designed photoreactor was barely capable to degrade any pollutant in water. After many trials and errors over a long period of time (months) the photoreactor successfully degraded 34% of methyl Orange ([MO] = 20 ppm) from 16 L volume in 34 hours of light irradiation. Aiming

to maximize the efficiency of the reactor, more changes were brought to its design. Along with the photocatalytic process, the electrolysis process was introduced into the photo-reactor. To incorporate electrolysis, the inner glass tube was replaced with a wire mesh cylinder. The photoreactor already had an external wire mesh cylinder. An external voltage was applied between the two-wire mesh cylinders to make them cathode and anode in the system. Either inner or outer wire mesh cylinder could potentially be anodic or cathodic.

To find the best suitable placement of the electrodes, two degradation experiments were done by switching the electrodes. In one of the experiments, a negative terminal of the DC source was connected to the central wire mesh and in another experiment, the central wire mesh was connected with the positive end of the DC source. To simplify the electrode connection type, the first set of connection types can be named forward and the second set as a reverse connection. For both experiments, an external voltage of 2.5 V was applied while the lamp was turned on for 24 hours.

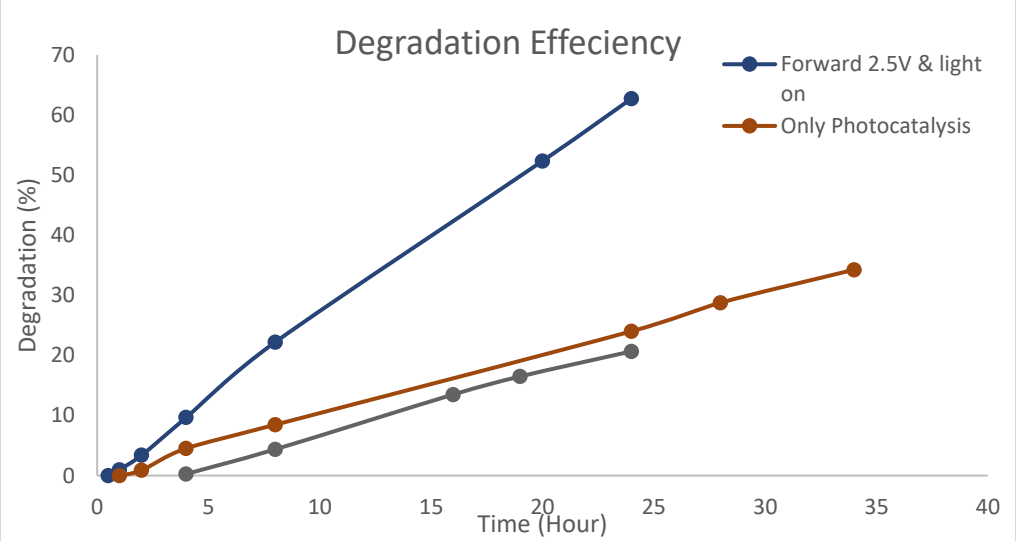

Figure 4.19 Degradation efficiency of photoreactor with only photocatalysis, 2.5 V forward and reverse with the light on. The degradation efficiency was measured using ppm of MO solution within 24-34 hours of reaction time.

In the first set of experiments with the forward connection, degradation was increased significantly compared to only photocatalysis experiments. About 40% of more pollutants degraded in 24 hours of reaction time. Whereas reduced degradation was observed if the electrodes were reversed connected. From this experiment, it was decided to continue the rest of the experiments with the forward connection. To find out the optimum potential of this experimental setup a series of degradation experiments were performed. In the first two sets of experiments, the applied voltage was set to 1.25V that is just above the water dissociation energy 1.23V [54] but, since the power supply didn't have the precision, the applied voltage was set to 1.3 V. The degradation efficiency of the pollutant was recorded about 24% by keeping the light off during 1.3 V which was about 5% less than the only photocatalysis. However, during 1.3 V with light, a 5% higher degradation efficiency was observed compared to only photocatalysis.

Another set of experiments applied 5 V with the light on and off, 10 V with the light on and finally 20 V light on. Maximum degradation of about 95% of the pollutant was achieved at 10V after 30 hours whereas applying 20V degradation was about 85% (Figure 4.20).

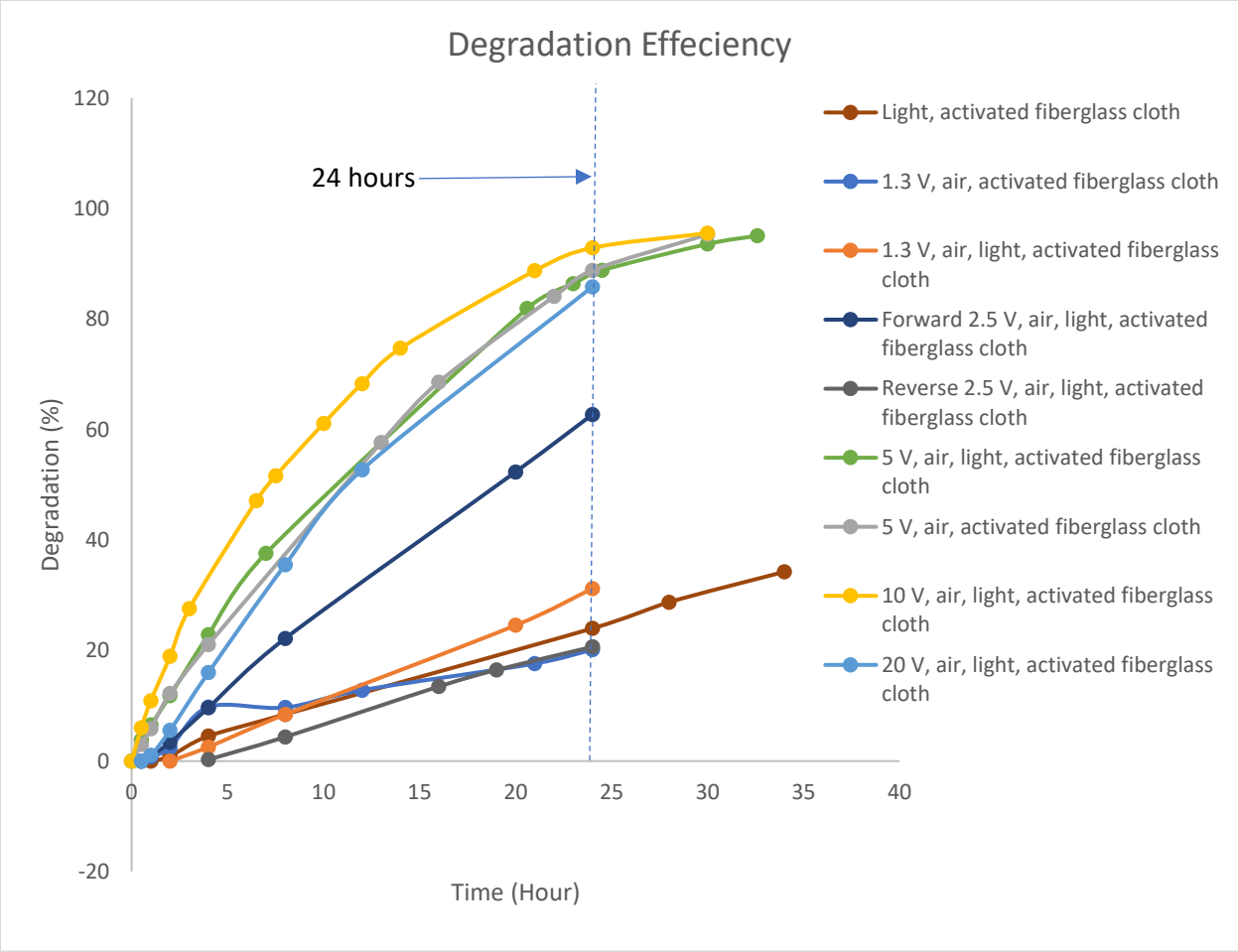

Figure 4.20 Degradation efficiency of the photoreactor under different conditions. The degradation efficiency was measured using 20 ppm of MO solution within 24 hours of reaction time.

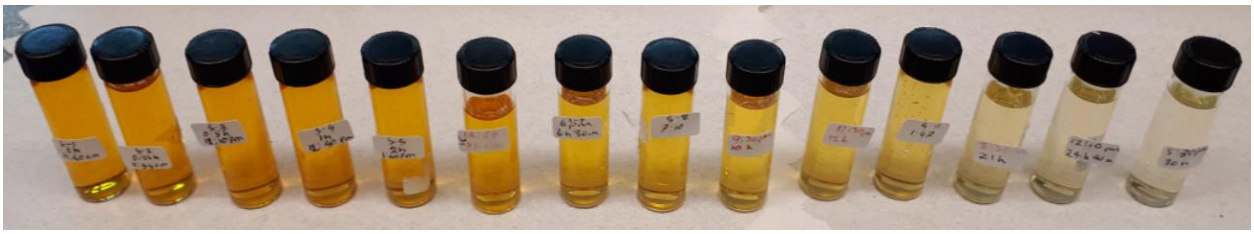

Figure 4.21 Change of pollutant concentration over 30 hours of treatment by the photoreactor. $[MO]^0$ = 20 ppm and applied potential difference =10V.

To better understand the electrolysis effect on this reactor and to choose the optimum voltage for the photoreactor, another graph was made showing the degradation versus applied voltage plotted

in Figure 4.23. From this graph, the increase in degradation as a function of voltage increases very steeply until 5V and then saturates at higher voltages.

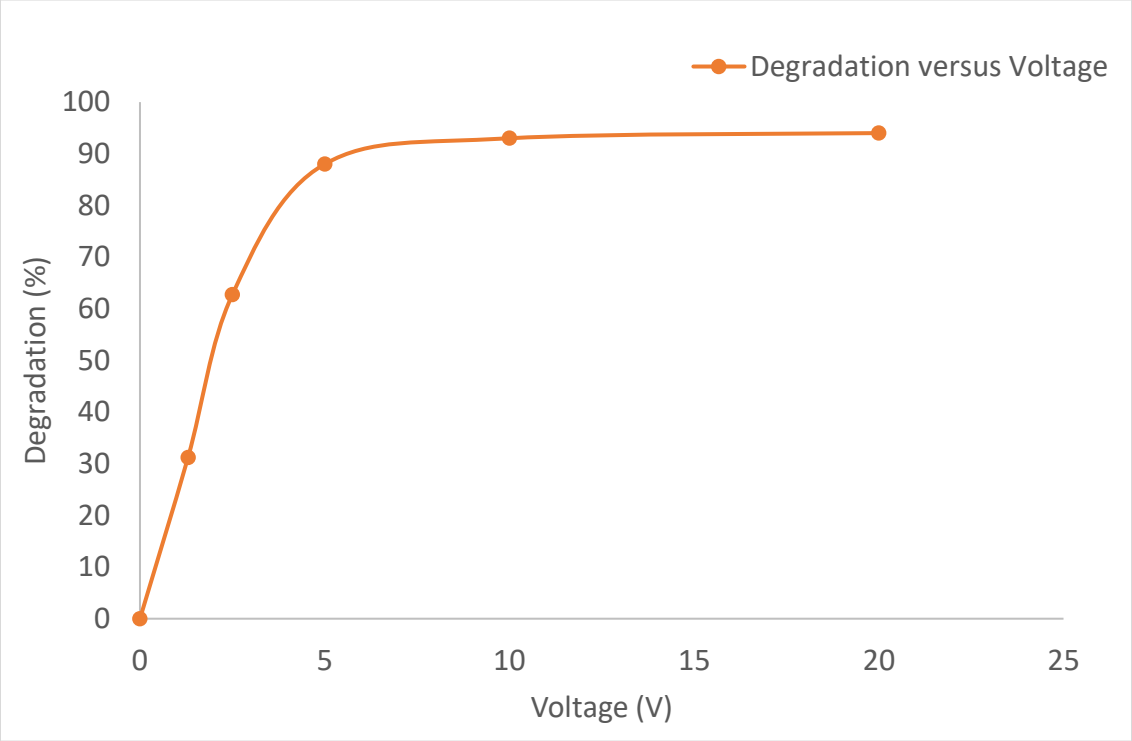

Figure 4.22 Degradation versus applied voltage of the photoreactor.

Considering the saturation at 5 V, two other degradation experiments were performed at 5 V and a comparative study was done by plotting them with other previous 5 V data. Here the contribution of only air is also plotted in this graph as a reference.

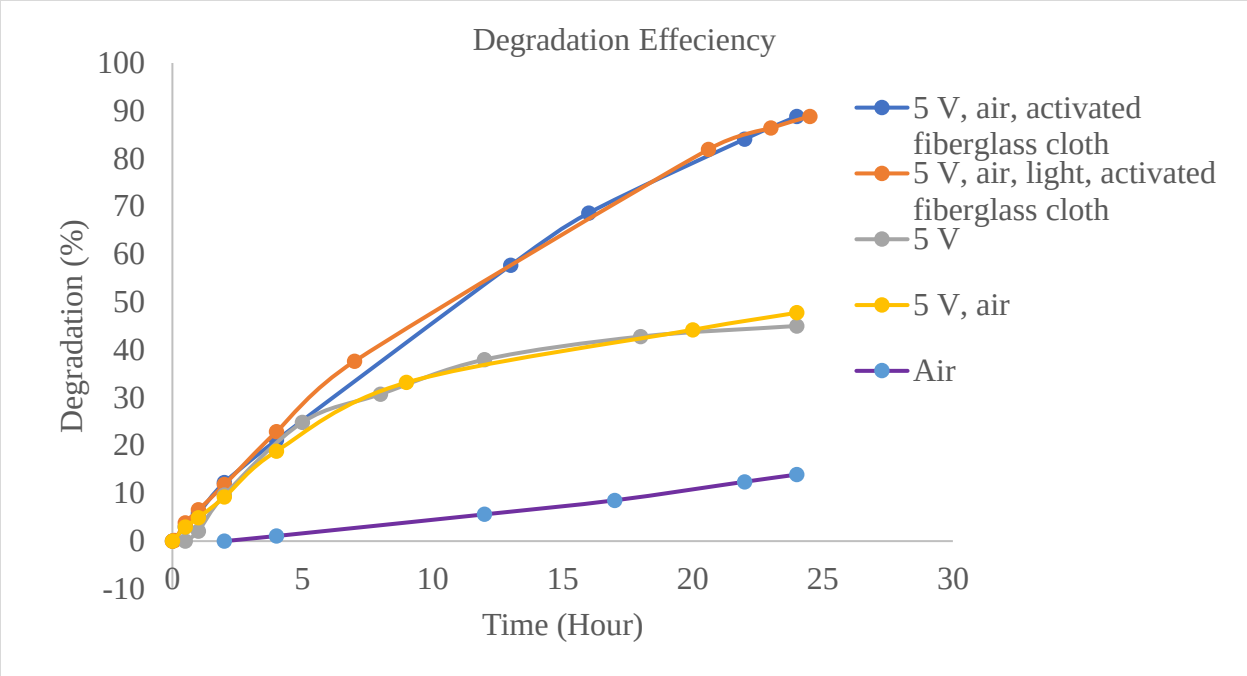

Figure 4.23 Degradation efficiency of the photoreactor at 5 V under different conditions where degradation of pollutants by only air is a reference. The degradation efficiency was measured using 20 ppm of MO solution within 24 hours of reaction time.

Chapter 5- Discussion

The revolutionary success for the addition of acid cleaning of the Fe doped TiO_2 crystals in the sol-gel crystal synthesis process made it possible to degrade 99.98% MO pollutant (with $[MO]_0$ = 20 mg/L, Catalyst load 500 mg/L) and 45% of Phenol pollutant (with $[Phenol]_0$ = 10mg/L, Catalyst load 500 mg/L) during 60 and 90 minutes of illumination period, respectively [8], [91]. With this rapid cleaning rate, I intended to apply this technology in a real wastewater cleaning reactor. Applying the crystals in a photoreactor without losing them to the environment was a challenge. Fiberglass cloth was chosen for some obvious reasons namely the high melting point of fiberglass cloth (1800°C) compared to the Fe-TiO_2 calcination temperature (400°C) and the cloth's flexibility to form almost any form. It was an ideal crystal immobilizing media for our purpose.

The experiments with the photoreactor were carried out by changing a parameter while holding other parameters constant. A remarkable change in degradation was observed when these parameters were varied. The parameters emphasized for photoreactor are described below:

Light:

Light is the main component to activate the crystals on fiberglass cloth to continue the photocatalysis. Even though the light alone was enough to activate the Fe-TiO_2 crystals in small scale water cleaning (such as 100 mL MO solution) to get ~100% pure water in 60 minutes, it did not work the same way for the photoreactor where a higher volume (16 L) of pollutant solution was treated. Only about 24% of degradation was achieved by the light in the photoreactor. The possible reasons could be as follows.

- In a 100 mL pollutant solution in a beaker, the crystals were agitated by a magnetic stirring bar throughout the entire pollutant solution. In this system, light-activated crystals could

freely travel across the pollutant dye molecules more effectively and degrade water pollutants more efficiently than the crystals attached to the fiberglass cloth.

- Again, as the Fe-TiO_2 nanocrystals were free to move in the 100 mL solution, no surface area was wasted due to their immobilization on the fiberglass cloth. the more the surface area exposed to the light, the more active will be the crystals to generate the $^{\bullet}OH$.
- Finally, 1.2 kW LED light not only emits light energy but also generated heat energy. This heat from the LED surfaces creates water vapor and slightly increased the pollutant concentration in the photoreactor. The inclusion of the heat exchanger around the photoreactor solved the heating issues.

Electrolysis Voltage:

By using light only in the photoreactor contributed very little to the cleaning of the wastewater because the ion current was possibly very low compared to the volume of the pollutant molecule concentration. To increase the ion current in the wastewater, different levels of voltage were applied in between the electrodes of the photoreactor. Application of an external voltage between the electrodes of the photoreactor increased the charge carriers in the wastewater that increased radicals that could be produced and hence the measured ion current increases.

It is observed in figure 4.2, with the increase of external voltage the rate of cleaning was improved. Also, from the graph, it is obvious that after 20 hours of pollutant degradation the rate of cleaning decreases. This can be explained for the early stage of cleaning as the pollutant concentration is high so that the pollutants easily reach the radicals produced around the active zone of a Fe-TiO_2 and get degraded as a result. But after 20 hours even with higher potentials like 20 V, the rate of cleaning decreases likely due to a lower pollutant concentration in the wastewater. With the decrease of the pollutant concentration, the distance between the pollutant molecules increases so

that fewer molecules travel to the active region of the photoactive crystal surface. It could also be due to the depletion of O_2 and OH^- in the water occurring during the degradation process.

Air:

In this photoreactor, air played a vital role in the degradation process. A continuous air-jet into the reactor kept a convective flow of pollutants in solution from inside to outside of the photoreactor through the activated fiberglass cloth enabling the pollutants to reach the crystals more readily.

Secondly, the air is another source of oxygen other than water. When the micro air bubbles reach the crystals, it creates a possibility to transform the oxygen molecules to superoxide radicals for cleaning purposes.

Finally, air-jet also acts as a heat exchanger. Direct airflow on the LED surface helped to keep the LED lamps cool possibly increasing their longevity.

Activated fiberglass cloth (Fe-TiO_2 crystals):

Although the acid-treated Fe-TiO_2 crystals alone showed a huge impact on a small scale (100 mL) wastewater cleaning process, its cleaning efficiency gets reduced by immobilizing Fe-TiO_2 on fiberglass cloth. But, the main purpose of immobilizing the Fe-TiO_2 crystals on fiberglass cloth was successful, so that no crystals gets loose in the environment. Moreover, fiberglass cloth is transparent to light and can be given any necessary shape for the reactor design.

Finally, it can be said that, for the sake of water cleaning, the drop in efficiency by immobilizing the Fe-TiO_2 on fiberglass cloth was not compromised. Instead, other parameters (external voltage, air) were introduced to ensure the high efficiency of the degradation of the pollutants.

Chapter 6- Future Work

The designed photoreactor is still in its very early stage, even though experimental results have been showing a very promising beginning. However, this research still needs to improve the photoreactor's degradation efficiency possibly by some modifications below:

- The photocatalytic part of the photoreactor is still lacking in full functionality. As the TiO_2 is a semiconductor material, heating the crystals could reduce the bandgap that could enable them to activate even in yellow light to increase the bandwidth of light absorption. To achieve this, a heating wire could be placed in between the activated fiberglass cloth just like the rear windshield of a car.
- An investigation could be done by changing the electrode's separation distance in the reactor and changing the electrode materials.
- A relatively smaller and modular photoreactor could be more effective to clean water.
- Along with wastewater cleaning, this photoreactor generates byproducts like H_2O, CO_2, H_2, N_2, etc. All the gases could be captured in reservoirs and used for different purposes such as extracted H_2 can be used in a fuel cell to regenerate the partial power of the photoreactor. CO_2 can be used in phytoplankton culture to grow phytoplankton to keep the ecosystem balanced and reduce the formation of red tides in the ocean.

References

[1] N. Riaz and M. Bustam, "Iron doped TiO 2 photocatalysts for environmental applications : fundamentals and progress," *Adv. Mater. Res.*, vol. Trans Tech, pp. 72–77, 2014.

[2] M. T. Amin, A. A. Alazba, and U. Manzoor, "A Review of Removal of Pollutants from Water/ Wastewater Using Different Types of Nanomaterials," *Adv. Mater. Sci. Eng.*, vol. 2014, 2014.

[3] N. J. Ashbolt, "Microbial contamination of drinking water and disease outcomes in developing regions," *Toxicology*, vol. 198, no. 1, pp. 229–238, 2004.

[4] G. Hutton, L. Haller, and J. Bartram, "Economic and health effects of increasing coverage of low cost household drinking-water supply and sanitation interventions to countries off-track to meet MDG target 10," 2007.

[5] T. Ali *et al.*, "Photocatalytic performance of Fe-doped TiO2 nanoparticles under visible-light irradiation," *Mater. Res. Express*, p. 015022, 2017.

[6] S. Sood, A. Umar, S. Kumar, and S. Kumar, "Highly effective Fe-doped TiO 2 nanoparticles photocatalysts for visible- light driven photocatalytic degradation of toxic organic compounds," *J. Colloid Interface Sci.*, vol. 450, pp. 213–223, 2015.

[7] S. Sood, A. Umar, S. K. Mehta, and S. K. Kansal, "Highly effective Fe-doped TiO2 nanoparticles photocatalysts for visible-light driven photocatalytic degradation of toxic organic compounds," *J. Colloid Interface Sci.*, vol. 450, pp. 213–223, 2015.

[8] V. Moradi, F. Ahmed, M. B. G. Jun, A. Blackburn, and R. A. Herring, "Acid-treated Fe-doped TiO2 as a high performance photocatalyst used for degradation of phenol under visible light irradiation," *J. Environ. Sci. (China)*, vol. 83, pp. 183–194, 2019.

[9] S. S. Turkar, D. B. Bharti, and G. S. Gaikwad, "Various methods involved in waste water treatment to control water pollution," *J. Chem. Pharm. Res*, vol. 3, no. 2, pp. 58–65, 2011.

[10] V. K. Gupta, I. Ali, T. A. Saleh, and S. Agarwal, "Chemical treatment technologies for waste-water recycling—an overview," *Rsc Adv.*, vol. 2, no. 16, pp. 6380–6388, 2012.

[11] M. I. Velasco, C. O. Kinen, R. Hoyos De Rossi, and L. I. Rossi, "A green alternative to synthetize azo compounds," *Dye. Pigment.*, vol. 90, no. 3, pp. 259–264, 2011.

[12] R. G. Saratale, G. D. Saratale, J. S. Chang, and S. P. Govindwar, "Bacterial decolorization and degradation of azo dyes: A review," *J. Taiwan Inst. Chem. Eng.*, vol. 42, no. 1, pp. 138–157, 2011.

[13] Y. Do Kim, J. H. Cho, C. R. Park, J. H. Choi, C. Yoon, and J. P. Kim, "Synthesis, application and investigation of structure-thermal stability relationships of thermally stable water-soluble azo naphthalene dyes for LCD red color filters," *Dye. Pigment.*, vol. 89, no. 1, pp. 1–8, 2011.

[14] A. A. M. Farag, A. M. Mansour, A. H. Ammar, and M. A. Rafea, "Characterization of electrical and optical absorption of organic based methyl orange for photovoltaic application," *Synth. Met.*, vol. 161, no. 19–20, pp. 2135–2143, 2011.

[15] A. Pandey, P. Singh, and L. Iyengar, “Bacterial decolorization and degradation of azo dyes,” *Int. Biodeterior. Biodegrad.*, vol. 59, no. 2, pp. 73–84, 2007.

[16] X. C. Jin, G. Q. Liu, Z. H. Xu, and W. Y. Tao, “Decolorization of a dye industry effluent by Aspergillus fumigatus XC6,” *Appl. Microbiol. Biotechnol.*, vol. 74, no. 1, pp. 239–243, 2007.

[17] H. Zollinger, *Colour Chemistry—Synthesis, Properties of Organic Dyes and Pigments*. 1987.

[18] J. S. Chang, T. S. Kuo, Y. P. Chao, J. Y. Ho, and P. J. Lin, “Azo dye decolorization with a mutant Escherichia coli strain,” *Biotechnol. Lett.*, vol. 22, no. 9, pp. 807–812, 2000.

[19] Philippe C. Vandevivere, Roberto Bianchi, and Willy Verstraete, “Treatment and reuse of wastewater from the textile wet-processing industry: Review of emerging technologies,” *J. Chem. Technol. Biotechnol.*, vol. 72, no. 4, pp. 202–289, 1998.

[20] J. Michałowicz and W. Duda, “Phenols - Sources and toxicity,” *Polish J. Environ. Stud.*, vol. 16, no. 3, pp. 347–362, 2007.

[21] J. T. Barber, H. A. Sharma, H. E. Ensley, M. A. Polito, and D. A. Thomas, “Detoxification of phenol by the aquatic angiosperm, Lemna gibba,” *Chemosphere*, vol. 31, no. 6, pp. 3567–3574, 1995.

[22] A. Maleki, A. H. Mahvi, and K. Naddafi, “C %" *% A :% a > D E c % 9 F ,*) 89 D ; ; I9 %; > $ A B,” pp. 19–24.

[23] D. Spangenberg, M. Schmitt, C. Ratzer, and K. Jochen, “The structure of phenol in the S_1 state determined by high resolution UV-spectroscopy,” *Chem. Phys.*, vol. 283, pp. 153–169, 2002.

[24] S. Mo, “Electronic and optical properties ofthree phases oftitanium dioxide: Rutile, anatase, and brookite,” vol. 51, no. 19, pp. 23–32, 1995.

[25] N. Cheremisinoff, Pen, *Handbook of water and Wastewater Treatment Technologies*. 2001.

[26] A. Latifossglu, A, G. Surucu, and M. Evirgen, “Water Pollut. IV: Model,” in *In Meas., Predict., 4th Int. Conf*, 1997, pp. 733–742.

[27] O. Sinev, I and S. Linevich, N, “Apparatus of flotation treatment of natural waters and wastewater,” *Izobreteniya*, vol. 26, pp. 369–370, 1997.

[28] M. T. Kato, J. A. Field, and G. Lettinga, “THE ANAEROBIC TREATMENT OF LOW STRENGTH WASTEWATERS IN UASB AND EGSB REACTORS,” *Water Sci. Technol.*, vol. 36, no. 6–7, pp. 375–382, 1997.

[29] C. Costa, M. C. Ma, and B. E. Barraga, “Biodegradation of azo dyes by bacteria inoculated on solid media,” vol. 75, pp. 73–81, 2007.

[30] C. Fux, M. Boehler, P. Huber, and I. Brunner, “Biological treatment of ammonium-rich wastewater by partial nitritation and subsequent anaerobic ammonium oxidation (anammox) in a pilot plant,” vol. 99, pp. 295–306, 2002.

[31] F. P. Van Der Zee and S. Villaverde, “Combined anaerobic – aerobic treatment of azo dyes — A short review of bioreactor studies,” vol. 39, pp. 1425–1440, 2005.

[32] A. R. Ribeiro, O. C. Nunes, M. F. R. Pereira, and A. M. T. Silva, “An overview on the advanced oxidation processes applied for the treatment of water pollutants de fi ned in the recently launched Directive 2013 / 39 / EU,” *Environ. Int.*, vol. 75, pp. 33–51, 2015.

[33] I. Levchuk, “Titanium Dioxide Based Nanomaterials for Photocatalytic Water Treatment,” *Acta Univ. Lappeenrantaensis*, 2016.

[34] M. Pelaez, N. Nolan, and M. Seery, “A Review on the Visible Light Active Titanium Dioxide Photocatalysts for Environmental Applications,” *Appl. Catal. B Environ.*, vol. 125, pp. 331–349, 2012.

[35] A. El-Kalliny, *Photocatalytic Oxidation in Drinking Water Treatment Using Hypochlorite and Titanium Dioxide*. 2013.

[36] S. Riyas, V. A. Yasir, and P. N. M. Das, “Crystal structure transformation of TiO 2 in presence of Fe 2 O 3 and NiO in air atmosphere,” vol. 25, no. 4, pp. 267–273, 2002.

[37] G. Zhang, Z. Sun, Y. Duan, R. Ma, and S. Zheng, “Synthesis of nano-TiO2/diatomite composite and its photocatalytic degradation of gaseous formaldehyde,” *Appl. Surf. Sci.*, 2017.

[38] A. R. Khataee and M. B. Kasiri, “Journal of Molecular Catalysis A : Chemical Photocatalytic degradation of organic dyes in the presence of nanostructured titanium dioxide : Influence of the chemical structure of dyes,” *"Journal Mol. Catal. A, Chem.*, vol. 328, no. 1–2, pp. 8–26, 2010.

[39] T. S. Emdal, “Characterization of photocatalytic materials used for water treatment,” 2015.

[40] J. E. S. Haggerty *et al.*, “High-fraction brookite films from amorphous precursors,” no. August, pp. 1–11, 2017.

[41] S. Malato, P. Fernández-Ibáñez, M. I. Maldonado, J. Blanco, and W. Gernjak, “Decontamination and disinfection of water by solar photocatalysis: Recent overview and trends,” *Catal. Today*, vol. 147, no. 1, pp. 1–59, 2009.

[42] B. Tryba, “Increase of the Photocatalytic Activity of TiO2 by Carbon and IronModification,” *Int. J. Photoenergy*, vol. 2008, 2008.

[43] A. Bahamonde, M. Ferna, and C. Ada, “Structure and activity of nanosized iron-doped anatase TiO 2 catalysts for phenol photocatalytic degradation,” *Appl. Catal. B Environ.*, vol. 72, no. 1, pp. 11–17, 2007.

[44] N. Riaz, F. K. Chong, B. K. Dutta, Z. B. Man, M. S. Khan, and E. Nurlaela, “Photodegradation of Orange II under visible light using Cu – Ni / TiO 2 : Effect of calcination temperature,” *Chem. Eng. J.*, vol. 185, pp. 108–119, 2012.

[45] K. Venkata, S. Rao, B. Lavédrine, and P. Boule, “Influence of metallic species on TiO 2 for the photocatalytic degradation of dyes and dye intermediates,” *J. Photochem.*

Photobiol. A Chem., vol. 154, no. 2, pp. 189–193, 2003.

[46] M. R. Hoffmann, S. T. Martin, W. Choi, and D. W. Bahnemannt, "Environmental Applications of Semiconductor Photocatalysis," *Chem. Rev.*, vol. 95, no. 1, pp. 69–96, 1995.

[47] E. Piera, M. I. Tejedor-tejedor, M. E. Zorn, and M. A. Anderson, "Relationship concerning the nature and concentration of Fe (III) species on the surface of TiO 2 particles and photocatalytic activity of the catalyst," *Appl. Catal. B Environ.*, vol. 46, no. 4, pp. 671–685, 2003.

[48] W. Choi, A. Termin, and M. R. Hoffmann, "The Role of Metal Ion Dopants in Quantum-Sized TiO2: Correlation between Photoreactivity and Charge Carrier Recombination Dynamics," *J. Phys. Chem.*, vol. 98, no. 51, pp. 13669–13679, 1994.

[49] S. Gelover, P. Mondragón, and A. Jiménez, "Titanium dioxide sol – gel deposited over glass and its application as a photocatalyst for water decontamination," *J. Photochem. Photobiol. A Chem.*, vol. 165, no. 1, pp. 241–246, 2004.

[50] N. Kieda and T. Tokuhisa, "Immobalization of TiO2 Photocatalyst Particls on Stainless Steel Substrates by Electrolytically Deposited Pd and Cu," vol. 45, pp. 42–45, 2006.

[51] J. Zeng, S. Liu, J. Cai, and L. Zhang, "TiO 2 Immobilized in Cellulose Matrix for Photocatalytic Degradation of Phenol under Weak UV Light Irradiation," *J. Phys. Chem. C*, vol. 114, no. 17, pp. 7806–7811, 2010.

[52] P. Lei *et al.*, "Immobilization of TiO 2 nanoparticles in polymeric substrates by chemical bonding for multi-cycle photodegradation of organic pollutants," *J. Hazard. Mater.*, vol. 227–228, pp. 185–194, 2012.

[53] U. Ibrahim and A. Halim, "Journal of Photochemistry and Photobiology C : Photochemistry Reviews Heterogeneous photocatalytic degradation of organic contaminants over titanium dioxide : A review of fundamentals , progress and problems," vol. 9, pp. 1–12, 2008.

[54] G. Gore, *Electrolytic Seperation, Recovery & Refining of Metals*. Watchmaker Publishing, 2003.

[55] K. Zeng and D. Zhang, "Recent progress in alkaline water electrolysis for hydrogen production and applications," *Prog. Energy Combust. Sci.*, vol. 36, no. 3, pp. 307–326, 2010.

[56] P. Yang, "A Constant Potential Molecular Dynamics Simulation Study of the Atomic-Scale Structure of Water Surfaces Near Electrodes," *Chinese J. Chem.*, vol. 37, no. 12, pp. 1251–1258, 2019.

[57] L. Chen, X. Dong, F. Wang, Y. Wang, and Y. Xia, "Base-acid hybrid water electrolysis," *Chem. Commun.*, pp. 4–7, 2016.

[58] F. Okada and K. Naya, *Electrolysis for ozone water production. In Electrlysis*. BOD-Books on Demand, 2012.

[59] H. Ito, T. Maeda, A. Nakano, and H. Takenaka, “Properties of Nafion membranes under PEM water electrolysis conditions,” *Int. J. Hydrogen Energy*, vol. 36, no. 17, pp. 10527–10540, 2011.

[60] J. Harju and A. Winnberg, “The distribution of OH in Taurus Molecular Cloud-1,” *Astron. Astrophys.*, vol. 353, pp. 1065–1073, 2000.

[61] P. Gehringer, *Radiation Processing of Aqueous Systems*. Oesterreichisches Forschungszentrum Seibersdorf, 1997.

[62] P. Englebienne, A. Van Hoonacker, and M. Verhas, “Surface plasmon resonance : principles , methods and applications in biomedical sciences,” vol. 17, pp. 255–273, 2003.

[63] K. L. Kelly, E. Coronado, L. L. Zhao, and G. C. Schatz, “Feature article,” pp. 668–677, 2003.

[64] B. Lamprecht, “Ultrafast plasmon dynamics in metal nanoparticles,” Karl-Franzens-Universität Graz, 2000.

[65] H. Jie, H. L. K. Chae, and J. Park, “by chemical vapor synthesis : band structure and photocatalytic activity under visible light,” pp. 1171–1180, 2012.

[66] G. Wu and A. Chen, “Direct growth of F-doped TiO 2 particulate thin films with high photocatalytic activity for environmental applications,” vol. 195, pp. 47–53, 2008.

[67] B. Jin, H. Bang, and K. S. Suslick, “Applications of Ultrasound to the Synthesis of Nanostructured Materials,” pp. 1039–1059, 2010.

[68] D. Qin *et al.*, “Facile Solvothermal Method for Fabricating Arrays of Vertically Oriented α -Fe 2 O 3 Nanowires and Their Application in Photoelectrochemical Water Oxidation,” pp. 5257–5263, 2011.

[69] Y. Wang, Y. He, Q. Lai, and M. Fan, “Review of the progress in preparing nano TiO2: An important environmental engineering material,” *JES*, 2014.

[70] V. Moradi, M. Jun, A. Blackburn, and R. Herring, “Significant improvement in visible light photocatalytic activity of Fe doped TiO2using an acid treatment process,” *Aplied Surf. Sci.*, 2017.

[71] “Lewco Speciality Products.” [Online]. Available: http://www.lewcospecialtyproducts.com/reinforcement-fabrics/Properties-of-Fiberglass-Fabrics. [Accessed: 17-Jan-2020].

[72] D. D. L. Chung, “Materials for thermal conduction,” *Appl. Therm. Eng.*, vol. 21, no. 16, pp. 1593–1605, 2001.

[73] Q. Zhang, L. Gao, and J. Guo, “Effects of calcination on the photocatalytic properties of nanosized TiO 2 powders prepared by TiCl 4 hydrolysis,” vol. 26, pp. 207–215, 2000.

[74] Y. You, S. Zhang, L. Wan, and D. Xu, “Applied Surface Science Preparation of continuous TiO 2 fibers by sol – gel method and its photocatalytic degradation on formaldehyde,” *Appl. Surf. Sci.*, vol. 258, no. 8, pp. 3469–3474, 2012.

[75] S. Koliyat, H. S. Kibombo, L. Mahoney, C. Wu, M. Yoon, and R. T. Koodali, “Synthesis of mixed phase anatase-TiO 2 (B) by a simple wet chemical method,” *Mater. Lett.*, vol. 95, pp. 175–177, 2013.

[76] P. K. Khanna, N. Singh, and S. Charan, “Synthesis of nano-particles of anatase-TiO 2 and preparation of its optically transparent film in PVA,” vol. 61, pp. 4725–4730, 2007.

[77] T. Y. Wei and C. C. Wan, “Heterogeneous Photocatalytic Oxidation of Phenol with Titanium Dioxide Powders,” *Ind. Eng. Chem. Res.*, vol. 30, no. 6, pp. 1293–1300, 1991.

[78] H. M. K. K. Pathirana and R. A. Maithreepala, “Photodegradation of 3,4-dichloropropionamide in aqueous TiO2 suspensions,” *J. Photochem. Photobiol. A Chem.*, vol. 102, no. 2–3, pp. 273–277, 1997.

[79] V. Augugliaro, V. Loddo, G. Marcì, L. Palmisano, and M. J. López-Muñoz, “Photocatalytic oxidation of cyanides in aqueous titanium dioxide suspensions,” *J. Catal.*, vol. 166, no. 2, pp. 272–283, 1997.

[80] N. Xu, Z. Shi, Y. Fan, J. Dong, J. Shi, and M. Z. C. Hu, “Effects of particle size of TiO2 on photocatalytic degradation of methylene blue in aqueous suspensions,” *Ind. Eng. Chem. Res.*, vol. 38, no. 2, pp. 373–379, 1999.

[81] T. Mason, *Practical Sonochemistry*. New York: Ellis Horwood, 1991.

[82] SantosHugo Miguel, *Ultrasound in chemistry: analytical applications*. KGaA, Weinheim: Wiley -Vch Verlag GmbH & Co, 2009.

[83] T. G. Leighton, *The Acoustic Bubble*. London, 1994.

[84] K. S. Suslick, *Sonochemistry*, 4th ed., vol. 26. New York: Jhon Wiley & Sons, Inc, 1998.

[85] S. J. Doktyez and K. S. Suslick, “interparticle collisions driven by ultrasound_Suslick_Science_1990.pdf,” *Sci. Reports*, vol. 2, no. 67, pp. 1987–1989, 1987.

[86] O’Lenick’ Anthony J, *Silicones for Personal Care*, 2nd ed. Allured Publishing Corporation, 2003.

[87] Z. Liu *et al.*, “Photocatalytic degradation of gaseous benzene with CdS-sensitized TiO 2 film coated on fiberglass cloth,” *J. Mol. Catal. A Chem.*, vol. 363–364, pp. 159–165, 2012.

[88] S. Lin, X. Zhang, Q. Sun, T. Zhou, and J. Lu, “Fabrication of solar light induced Fe-TiO2 immobilized on glass-fiber and application for phenol photocatalytic degradation,” *Mater. Res. Bull.*, vol. 48, no. 11, pp. 4570–4575, 2013.

[89] G. Jiang *et al.*, “Immobilization of N, S-codoped BiOBr on glass fibers for photocatalytic degradation of rhodamine B,” *Powder Technol.*, vol. 261, pp. 170–175, 2014.

[90] W. Liu, L. Zhang, L. X. Cao, G. Su, and Y. G. Wang, “Glass fibers templated preparation of TiO2 microtubes assembled from nano/micro hierarchical TiO2 crystals,” *J. Alloys Compd.*, vol. 509, no. 7, pp. 3419–3424, 2011.

[91] V. Moradi, M. B. G. Jun, A. Blackburn, and R. A. Herring, “Significant improvement in

visible light photocatalytic activity of Fe doped TiO 2 using an acid treatment process," *Appl. Surf. Sci.*, vol. 427, pp. 791–799, 2018.